Design-to-Device Approach Affords Panchromatic Co-sensitized Solar Cells

Christopher B. Cooper[1,2,3], Edward J. Beard[1], Dr. Álvaro Vazquez-Mayagoitia[4], Dr. Liliana Stan[4], Dr. Gavin B. G. Stenning[5], Dr. Daniel W. Nye[5], Julian A. Vigil[6], Tina Tomar[7], Jingwen Jia[8], Dr. Govardhana Babu Bodedla[9], Dr. Song Chen[9], Lucía Gallego Aibar[10], Dr. Santiago Franco Ontaneda[10], Dr. Antonio Carella[11], Dr. K.R. Justin Thomas[7], Dr. Song Xue[8], Dr. Xunjin Zhu[9], Dr. Jacqueline M. Cole,[1,2,3,4,5*]

[1]Cavendish Laboratory, Department of Physics, University of Cambridge, J. J. Thomson Avenue, Cambridge, CB3 0HE, UK
[2]Department of Chemical Engineering and Biotechnology, University of Cambridge, West Cambridge Site, Philippa Fawcett Drive, Cambridge, CB3 0AS, UK
[3]Research Complex at Harwell, Rutherford Appleton Laboratory, Harwell Oxford, Didcot, Oxon, OX11 0FA, UK
[4]Argonne National Laboratory, 9700 South Cass Avenue, Argonne, IL 60439. United States.
[5]ISIS Neutron and Muon Facility, STFC Rutherford Appleton Laboratory, Harwell Science and Innovation Campus, Didcot, OX11 0QX, UK
[6]Department of Chemistry, University of Cambridge, Lensfield Rd, Cambridge, CB2 1EW, UK
[7]Organic Materials Laboratory, Department of Chemistry, Indian Institute of Technology Roorkee, Roorkee – 247667, India
[8]Tianjin Key Laboratory of Organic Solar Cells and Photochemical Conversion, School of Chemistry & Chemical Engineering, Tianjin University of Technology, 391 Binshui Xidao, Xiqing District Tianjin 300384, P.R. China
[9]Department of Chemistry and Institute of Molecular Functional Materials, Hong Kong Baptist University, Kowloon Tong, Hong Kong, China
[10]Departamento de Química Orgánica, ICMA, Universidad de Zaragoza-CSIC, 50009 Zaragoza, Spain.
[11]Department of Chemical Sciences, University of Naples Federico II, Via Cintia 21, 80126, Naples, Italy

*Author for correspondence (E-mail: jmc61@cam.ac.uk)

Abstract

Data-driven materials discovery has become increasingly important in identifying materials that exhibit specific, desirable properties from a vast chemical search space. Synergic prediction and experimental validation are needed to accelerate scientific advances related to critical societal applications. We report a design-to-device study that uses high-throughput screens with algorithmic encodings of structure-property relationships, to identify new materials with panchromatic optical absorption, whose photovoltaic device applications are then experimentally verified. Our data-mining methods sourced 9,431 dye candidates, which were auto-generated from the literature using a custom text-mining tool. These candidates were sifted via a data-mining workflow that was tailored to identify optimal combinations of organic dyes that have complementary optical absorption properties such that they can harvest all available sunlight when acting as co-sensitizers for dye-sensitized solar cells (DSSCs). Six promising dye combinations were short-listed for device testing, whereupon one dye combination yielded co-sensitized DSSCs with power conversion efficiencies comparable to those of the high-performance, organometallic dye, N719. These results demonstrate how data-driven molecular engineering can accelerate materials discovery for panchromatic photovoltaic or other applications.

1. Introduction

Data-driven materials discovery[1,2] allows researchers to mine a vast chemical search space and identify materials that exhibit specific, desirable properties. These high-throughput, automatic approaches have accelerated scientific discovery in important research areas such as photovoltaics, water splitting, and gas capture.[3–9] This paper presents and utilizes a materials discovery approach to predict and then experimentally realize panchromatic solar cells, a factor critical to photovoltaic performance.[10–12]

The approach exploits co-sensitization, in the field of dye-sensitized solar cells (DSSCs), which offers a promising means to achieve the desired panchromatic solar cells for a variety of applications. DSSCs can exhibit efficiencies as high as 28.9% in ambient lighting, outperforming GaAs devices.[13] Their transparency makes DSSCs optimal devices for solar windows,[14] while their ability to be fabricated on flexible substrates or as fibers enables passive energy harvesting in wearable devices and textiles.[15–18] DSSCs can also be manufactured at low-cost using scalable techniques such as roll-to-roll processing[19], inkjet printing[20], and ultrafast sensitization[21,22], which are necessary to reach competitive price-to-performance ratios.

Thus far, co-sensitization has helped afford the world-record DSSC efficiency of over 14% under full illumination;[23] however, the lack of a rational, automated method to select combinations of dyes from a large database of light-harvesting chromophores limits further progress. Despite numerous computational studies complementing experimental work on singly-sensitized DSSCs, only a few studies have attempted to computationally predict and analyse co-sensitized

DSSCs;[24–27] and up until now, no study has offered a full design-to-device materials discovery approach for co-sensitized DSSCs. This paper presents and validates such a method.

A database of dye candidates was compiled via automated text-mining of published journal articles. This custom-made database was then mined using high-throughput screening methods which employed algorithmic encodings of structure-property relationships to identify five promising organic dyes that could act together as co-sensitizers, with six possible co-sensitization pairings. The predicted dyes, which had never been co-sensitized, were then synthesized and characterized experimentally. The dye combination that performed best within a DSSC device exhibited a power conversion efficiency that is comparable to that of the high-performance, organometallic dye, N719. Furthermore, surface characterization via atomic force microscopy (AFM) and x-ray reflectometry (XRR) provided, for the first time, a quantitative analysis of how co-sensitization affected dye aggregation and adsorption onto TiO_2. These results offer a promising example of how a materials discovery approach can accelerate and improve scientific advances related to panchromatic solar cells or other applications.

2. Results and Discussion

2.1. Materials Prediction of Co-sensitizers

Figure 1 provides a schematic of the computational workflow that predicts optimal dye combinations for co-sensitization. First, we auto-generated a database of 9,431 dye candidates (including their chemical structure, maximum absorption wavelengths, and molar extinction coefficients) from academic literature, using the text-mining software ChemDataExtractor.[28]

Initial screens then removed small molecules, organometallic dyes, and chemicals not absorbing in the solar spectrum, leaving 3,053 organic dyes remaining.

Second, we screened dyes based on two key structure-property relationships: the presence of a carboxylic acid group and a sufficiently large molecular dipole moment. The former ensures that the selected dyes contain a high-performance DSSC anchoring group[29] which enables them to effectively adsorb onto TiO_2 surfaces to create working electrodes. The latter is required for effective intramolecular charge transfer after photoexcitation. After selecting only dyes with carboxylic acid groups via substructure searching and eliminating dyes with a molecular dipole moment less than 5 Debye,[30] 309 dyes remained in the shortlist.

Next, we employed an algorithm to predict dye combinations for co-sensitization based on their optical absorption properties. We provide an overview here with full details given in the Supporting Information. Using the maximum absorption wavelengths and extinction coefficients gathered by ChemDataExtractor,[28] we ranked each potential dye combination using a quality score. Algorithm metrics producing a high quality score comprised a large overlap factor, absorption fraction, and relative change. These ensured that the dye combination (i) did not have significant optical absorption overlap between dyes, (ii) exhibited panchromatic absorbance, and (iii) improved significantly from the addition of each dye. This yielded a shortlist of 33 dyes.

We then checked the HOMO – LUMO energy levels of the 33 short-listed dyes using Density Functional Theory (6311G** basis set and B3LYP functional) to confirm that the LUMO energy levels were greater than that of the conduction band edge of anatase TiO_2 (-3.74 eV vs.

vacuum)[31] and that the HOMO energy levels were below the redox potential of I^-/I_3^- (-4.85 eV vs. vacuum).[32] These are necessary energetic properties for device integration into a standard DSSC, though these checks could be modified for integration with other semiconductors or redox couples. This screen reduced the shortlist to 29 dyes.

From here, we manually evaluated each dye and considered practical constraints such as ease of synthesis or availability. This afforded a set of five dyes for experimental validation: C1,[33] 8c,[34] XS6,[35] 15,[36] and H3.[37] **Figure 2** provides the 2D and 3D chemical structures of the dyes, with molecular dimensions annotated as a reference for the surface characterization work discussed later. The maximum optical absorption wavelengths and corresponding molar extinction coefficients were 457 nm (1.00×10^5 L mol^{-1} cm^{-1}), 414 nm (3.27×10^4 L mol^{-1} cm^{-1}), 432 nm (1.25×10^5 L mol^{-1} cm^{-1}), 573 nm (3.36×10^4 L mol^{-1} cm^{-1}), and 585 nm (2.87×10^4 L mol^{-1} cm^{-1}), for dyes C1, 8c, XS6, 15, and H3, respectively.[33–37] Co-sensitizing any of the first three dyes (C1, 8c, and XS6) with either of the last two dyes (15 and H3) should create DSSCs with broad optical absorbance.

2.2 Experimental Validation of Predicted Dyes

We experimentally validated and characterized these six potential co-sensitizations using UV-vis absorption spectroscopy and photovoltaic device testing. **Figure 3A** gives the optical absorption spectrum of each individual dye in dichloromethane (DCM). The dyes absorb throughout the visible spectrum, with C1, 8c, and XS6 absorbing primarily in the 300-500 nm range; 15 absorbing primarily in the 500-700 nm range; and H3 exhibiting broad absorbance with a gap between 425-525 nm. **Figure 3B** gives the optical absorption spectra of each dye adsorbed onto

TiO_2. Both C1 and 8c exhibit wider optical absorption spectra compared to their absorbance in DCM while 15 and H3 display a 52 and 26 nm blue shift in maximum absorbance, respectively.

For each dye combination, we identified a sequential and cocktail method that afforded co-sensitized working electrodes (WE) with panchromatic optical absorption (see **SI Table 1**). Samples fabricated via the sequential and cocktail method are referred to as "*Dye 1 then Dye 2*" and "*Dye 1 and Dye 2*," respectively. For simplicity, we use these sample names throughout the letter to refer to WEs sensitized under the specific conditions described in **SI Table 1**. Compared to the spectra of the individual dyes on TiO_2, the co-sensitized WEs exhibit broad absorbance throughout the visible region (400-700 nm), indicating that adsorption of both dyes onto TiO_2 has been achieved (see **SI Fig. 1**). We found that C1 significantly desorbs 15, and thus, we adjusted each sensitization method to achieve adequate adsorption of both dyes (see **SI Fig. 2**).

We then tested the photovoltaic performance of singly-sensitized and co-sensitized DSSCs compared to a reference sample sensitized with the organometallic N719 dye. Reporting with the η_{dye}: η_{N719} ratio method permits effective comparison between power conversion efficiencies, η, published in the literature under a range of experimental conditions. This method has already been adopted in over 250 journal articles.[38] **SI Table 2** provides the photovoltaic device performance for each sample, averaged across three different DSSCs. All measured J-V curves are given in **SI Figure 3**.

Figure 3C presents the J-V curve for the best-performing co-sensitization, *XS6 and 15*, which exhibited a 38% increase in η compared to the corresponding singly-sensitized DSSCs.

Moreover, its $\eta_{dye}:\eta_{N719}$ ratio of 0.92 demonstrates performance comparable to that of the high-performance, organometallic N719 dye. Similarly, *XS6 then 15* increased η by 23%, obtaining a promising $\eta_{dye}:\eta_{N719}$ ratio of 0.82. Both *XS6 and 15* and *XS6 then 15* exhibit high open circuit voltages (V_{oc}) of 700 and 685 mV, respectively, indicating that electron recombination has been minimized. *XS6 and 15* achieves a higher short-circuit current density (J_{sc}) than *XS6 then 15*, 6.5 mA cm^{-2} compared to 5.5 mA cm^{-2}. Comparing the UV-vis absorption spectra of *XS6 then 15* and *XS6 and 15* (**Fig. 3D**) suggests that the increase in J_{sc} arises from the adsorption of more molecules of 15 to TiO_2 achieved via the cocktail approach.

C1 then 15 and *C1 and 15* showed a modest, but not statistically significant, gain in η from co-sensitization, 6% and 7%, respectively, with $\eta_{dye}:\eta_{N719}$ ratios of 0.54. Both 8c and H3 afforded dramatically lower J_{sc} values and slightly lower V_{oc} values than the other dyes when singly sensitized, leading to deleterious effects whenever they were co-sensitized. Calculated HOMO and LUMO energy levels for these dyes show that 8c and H3 have the lowest predicted LUMO energy levels and highest predicted HOMO energy levels. These smaller band gaps imply lower driving forces for electron injection and dye regeneration, possibly explaining their poorer performance.

2.3 Surface Characterization of Co-sensitized DSSCs

To better understand the molecular origins of these photovoltaic results, we characterized the surface structure of singly-sensitized and co-sensitized WEs, using atomic force microscopy (AFM) and x-ray reflectometry (XRR). While previous studies have used either AFM or XRR to determine dye aggregation effects, dye coverage, inter-dye spacing, and dye-layer thicknesses in

singly-sensitized DSSCs,[39–41] this letter presents the first study of AFM or XRR on co-sensitized WEs and provides a quantitative analysis of how co-sensitization affects dye aggregation and adsorption onto TiO_2.

We selected an AFM base height of 3 nm as the dye aggregation threshold, since this is greater than the molecular length of any dye (**Figure 2**). Thereby, any continuous areas greater in height than this threshold were classified as aggregates in the AFM images. For each sample, we obtained five distinct 20 x 20 μm AFM images (see representative images in **Fig. 4**) and characterized the aggregates based on mean height, max height, coverage, and number of aggregates (**Table 1**).

Co-sensitized WEs, *XS6 then 15*, *XS6 and 15*, *XS6 then H3*, and *XS6 and H3* exhibited the lowest amount of dye aggregation with low aggregate coverage (0.3 - 0.7%) and low total numbers of aggregates (0.2-0.8 per μm). *XS6 and 15* specifically exhibited aggregate coverage of 0.3% and 0.2 aggregates per μm, both an order of magnitude lower than the aggregation observed in 15 only. The minimal aggregation exhibited by *XS6 then 15* and *XS6 and 15* suggests that a dye monolayer has formed on TiO_2 and partially explains their optimal photovoltaic performance. Similarly, both *C1 then 15* and *C1 and 15* exhibited less aggregation than their singly-sensitized counterparts.

Overall, co-sensitized WEs show reduced aggregation compared to their singly-sensitized counterparts for seven out of twelve samples. C1, 8c, and 15 singly-sensitized WEs all show significant aggregation whose coverages are 3%, 3%, and 7%, respectively. C1 and 8c display

many small aggregates manifested by the low mean and max heights (5-7 nm) and high numbers of aggregates (2-3 per μm^2); this indicates that the dyes aggregate longitudinally (i.e. side-by-side). In contrast, 15 exhibits relatively large aggregates with higher mean height (8 nm) and max height (15 nm) but a lower number of aggregates (1.1 per μm^2), suggesting a combination of both longitudinal and lateral (i.e. stacked) dye aggregation. Both XS6 and H3 show minimal aggregation, with aggregate coverages of 1% and 0.3%, respectively, and a low total number of aggregates (0.2-0.3 per μm^2). For XS6, this minimal aggregation could arise from its twisted π-conjugation, while for H3 it could result from the bulky hexyloxy chains. Both of these properties have reduced the aggregation of other dye molecules.[42]

Next, we employed XRR to obtain structural information about the adsorbed dye layer. Fitting data collected from each WE to a model based on calculated molecular dimensions and scattering length densities (SLDs) (**SI Table 3**) revealed estimates of the dye-layer thickness, SLD_{dye}, surface roughness, and surface coverage (**Table 1**). Additional fitted parameters, all raw data and fitted models, and all calculations are given in the Supporting Information.

Co-sensitized WEs *XS6 then 15* and *XS6 and 15* exhibit low dye-layer thicknesses (19 Å) together with high surface coverages (above 70%). Consistent with the minimal aggregation seen in the corresponding AFM images, these results strongly suggest the formation of a tightly-packed monolayer on the TiO_2 surface, corroborated by the high V_{oc} of both dye combinations (> 685 mV). Relatively poor surface coverage (49% and 52%) is observed in *C1 then 15* and *C1 and 15*, which are the other DSSCs to prospect any gain in η from co-sensitization (**SI Table 2**).

In common with the AFM results, XRR models for *XS6 then H3* and *XS6 and H3* display some of the lowest dye-layer thicknesses (21-22 Å) and highest surface coverages (>70%), despite their poor photovoltaic performance. Additionally, singly-sensitized XS6 and H3 working electrodes have thicknesses near their molecular lengths, indicating that they have formed monolayers on the TiO_2 surface. We calculated the intermolecular spacing in the XS6 and H3 dye monolayers to be 3.7 and 2.8 Å, respectively, implying each present a tightly-packed monolayer that prevents I_3^- (molecular length of ~5.28 Å) from reaching the TiO_2 surface to cause electron recombination issues (see Supporting Information).[40] The high surface coverage (73%) and V_{oc} (730 mV) observed for XS6, the highest of the singly-sensitized dyes in both cases, corroborates the idea of a packed monolayer. The inferior photovoltaic performance of H3, despite its minimal aggregation in AFM images (0.3%), low intermolecular spacing (2.8 Å), and high surface coverage (62%), suggests poor electron injection by H3 into TiO_2.

3. Conclusions

In this work, we have presented and experimentally validated a design-to-device approach that employs structure-property relationships in a computational workflow to achieve panchromatic solar cells. The results, especially for *XS6 then 15* and *XS6 and 15*, offer a promising example of accelerated materials discovery for photovoltaics, given that they yield power conversion efficiencies which are comparable to that of N719, the high-performance organometallic dye that acts as the industry standard for DSSCs. This accomplishment is despite having deliberately restricted our search to organic dyes that historically produce lower DSSC efficiencies but are environmentally superior. This demonstrates the power of our approach.

Our work thus offers a rare example of a full cycle of data-driven materials discovery, which is difficult to achieve owing to a dearth in demonstrable methods. Moreover, our methods are distinguished by their success, showing that co-sensitization of DSSCs can be tailored rationally to afford solar-cell devices that perform to world-recognized photovoltaic standards.

4. Experimental Section

4.1 Assembly of the Parent Database

The text-mining software tool, ChemDataExtractor,[28] was used to auto-generate a custom database of dye candidates for this project by sourcing matched quantities of {chemical, optical absorption properties} from the academic literature. Each data field comprises the chemical structure of a molecule in simplified molecular-input line-entry system (SMILES) format[43] along with its optical absorption peak wavelength, λ_{max}, and molar extinction coefficients, ε. SMILES were resolved from their chemical names using OPSIN[44] while OpenBabel[45] was used to read the SMILES structure of each chemical molecule and check for duplicates. After narrowing the shortlist to 309 dyes (i.e. prior to implementing the dye matching algorithm), manual verification of the maximum absorption peak wavelength and molar extinction coefficient for each short-listed dye was completed and erroneous data were corrected. Data auto-extraction employed the supercomputing resources at the Argonne Leadership Computing Facility, USA.

4.2 Initial Screens and Identification of Suitable Anchoring Group

The RDKit library[46] in Python was utilized for basic filtering of the dye candidates (i.e. removal of small molecules or organometallic dyes). Molecules without a maximum absorption peak

between 350-1000 nm were removed. RDKit was also used for substructure searching in which only dyes with an identified carboxylic acid group (COOH) in their structure were kept.

4.3 Molecular Dipole Moment Calculations

To accurately estimate the molecular dipole moment of each dye candidate in a computationally efficient manner, 3D coordinates were generated for each dye candidate from its corresponding SMILES structure via a weighted rotor search (as defined in OpenBabel) to identify five low-energy conformers. The geometries of the five selected conformers were then further optimized using PM7 semi-empirical geometry optimization executed in MOPAC.[47] PM7 was selected due to its previous use with organic molecules.[48] The molecular dipole moment of each dye was taken from the PM7 results of the lowest energy conformer.

4.4 HOMO/LUMO Energy Level Calculations

HOMO and LUMO energy levels were estimated for each remaining dye candidate using a single point calculation with Density Functional Theory (DFT) with the 6311G** basis set and B3LYP functional on the previously PM7-optimized geometry of the lowest energy conformer to reduce computational cost.[49–51] All DFT calculations were completed using NWChem software via the supercomputing resources at the Argonne Leadership Computing Facility, USA.[52]

4.5 Dye Synthesis and Characterization

The research groups who originally made each dye synthesized the predicted dyes as a collaboration specifically for this project, according to their previously reported methods.[33–37] Reproducibility was verified for each dye by nuclear magnetic resonance (NMR) spectroscopy.

^{1}H NMR spectra were recorded on a Bruker 400 MHz DCH cryoprobe spectrometer at room temperature. Chemical shifts for ^{1}H spectra are referenced to residual signals from the deuterated solvent.

C1. ^{1}H NMR (DMSO-d_6, 400 MHz): δ/ppm = 12.27 (bs, 1H), 8.72 (s, 2H), 8.52 (s, 2H), 8.03-7.96 (m, 4H), 7.88-7.83 (m, 2H), 7.81 (s, 1H), 7.77 (s, 1H), 7.73-7.68 (m, 2H), 7.66-7.61 (m, 2H), 7.43 (bs, 1H), 7.39 (bs, 1H), 6.84-6.81 (m, 2H), 6.57 (d, J = 15.6 Hz, 2H), 4.37-4.29 (m, 4H), 2.05-1.97 (m, 2H), 1.40-1.12 (m, 16H), 0.87 (t, J = 7.2 Hz, 6H), 0.78 (t, H = 7.2 Hz, 6H).

8C. ^{1}H NMR (DMSO-d_6, 400 MHz): δ/ppm = 8.43 (s, 1H), 7.95 (d, J = 3.9 Hz, 1H), 7.75-7.70 (m, 2H), 7.66-7.63 (m, 1H), 7.62-7.58 (m, 1H), 7.57-7.53 (m, 1H), 7.52-7.48 (m, 1H), 7.39-7.36 (m, 1H), 7.23-7.20 (m, 1H), 7.17-7.13 (m, 1H), 4.31 (m, 2H), 1.50-1.39 (m, 2H), 1.11-0.99 (m, 2H), 0.66 (t, J = 7.4 Hz, 3H).

XS6. ^{1}H NMR (DMSO-d_6, 400 MHz): δ/ppm = 8.00 (s, 1H), 7.86 (d, J = 8.8 Hz, 2H), 7.66 (m, 2H), 7.48-7.39 (m, 4H), 7.26-7.08 (m, 9H), 6.99-6.92 (m, 4H), 6.78 (s, 1H), 6.74-6.71 (m, 2H), 6.70-6.66 (m, 2H), 2.93 (s, 6H), 2.91 (s, 6H).

15. ^{1}H NMR (THF-d_8, 400 MHz): δ/ppm = 8.28 (s, 1H), 8.02-7.97 (m, 2H), 7.88-7.84 (m, 2H), 7.78 (s, 1H), 7.76-7.72 (m, 4H), 7.56-7.37 (m, 13H), 6.75 (bd, J = 2.0 Hz, 1H), 6.12 (s, 1H), 4.87 (s, 2H), 1.09 (s, 9H).

H3. ^{1}H NMR (DMSO-d_6, 400 MHz): δ/ppm = 8.81 (s, 1H), 8.65 (d, J = 4.1 Hz, 1H), 8.37 (s, 1H), 8.00 (d, J = 4.1 Hz, 1H), 7.98-7.94 (m, 2H), 7.13-7.08 (m, 4H), 6.97-6.92 (m, 4H), 6.90-6.86 (m, 2H), 3.95 (t, J = 6.5 Hz, 4H), 1.75-1.67 (m, 4H), 1.46-1.38 (m, 4H), 1.36-1.26 (m, 8H), 0.88 (t, J = 7.0 Hz, 6H).

4.6 UV-vis Absorption Spectroscopy

The optical absorption spectra of the fabricated WEs (see Supporting Information for fabrication details) and of the prepared dye solutions (in DCM, 3 x 10^{-5} M) were acquired using a Shimadzu UV-1800 Spectrophotometer. All solutions were tested in 10 mm pathlength quartz precision cells (SUPRASIL, Hellma Analytics).

4.7 Photovoltaic Performance Testing

The current-voltage characteristics of the singly-sensitized and co-sensitized DSSCs (see Supporting Information for fabrication details) were measured with an Ivium CompactStat potentiostat under constant illumination by a Newport Oriel Xenon 150 W solar light simulator (100 mW cm^{-2}, AM1.5G and IR water filters, $\lambda < 400$ nm), calibrated with a Newport Optical power meter (Model 1916-R). Solar cells had an active area of 0.30 cm^2 and were masked with an 8 x 8 mm aperture. Linear scanning voltammetry was performed at room temperature in ambient air at 50 mV s^{-1} with a 5 s equilibrium time between forward and backward scans. No pre-conditioning of the devices was completed.

Using the measured J-V curves, the short-circuit current density (J_{sc}), open-circuit voltage (V_{oc}), and fill-factor (FF) were determined for each fabricated cell. The photovoltaic efficiency of the cell was then calculated by:

$$\eta = \frac{J_{sc} * V_{oc} * FF}{P_{in}} \quad (1)$$

where P_{in} is the power of incident-light radiation. Reported DSSC parameters were found by averaging across 3 individually tested cells. For co-sensitized DSSCs, we calculated the percentage change in efficiency by comparing each co-sensitized DSSC to the best performing singly-sensitized DSSC of the dyes used. The J-V curves for all tests are given in **SI Figure 3**.

4.8 Atomic Force Microscopy (AFM)

The surfaces of singly-sensitized and co-sensitized WEs (see Supporting Information for fabrication details) were imaged using a Bruker Dimension 3100 Atomic Force Microscope with a monolithic silicon AFM probe (Tap300-G, Budget Sensors) with a tip radius less than 10 nm, a resonance frequency of 300 kHz, and a force constant of 40 N/m. Tapping mode was used to produce five 20 x 20 μm images of different areas of each sample to ensure a representative measurement. All AFM images were processed using Gwyddion software.[53] All AFM images are given at the end of the Supporting Information.

4.9 X-Ray Reflectometry (XRR)

A Rigaku SmartLab X-Ray Diffractometer equipped with a 9 kW rotating anode with a Cu X-ray source (λ = 1.54Å) and Ge (220x2) monochromator was utilized to take XRR measurements.

Data were collected from 0.1° to 10° at a speed of 0.25° per minute with a 0.02° step size. The GenX reflectivity software package was used to analyze the data and fit the structural parameters.[54] Similar to previous studies,[40,41] a three-layer approach of native silicon oxide, TiO_2, and dye was employed to fit the XRR data. To minimize the number of parameters fit in the model, the thickness and scattering length density (SLD) of the native oxide layer were fixed at 5 Å and 18.9 x 10^{-6} $Å^{-2}$, respectively. The substrate of the model was Si wafer with a constant SLD of 20.1 x 10^{-6} $Å^{-2}$. Errors were calculated based on the change in parameter needed to result in a greater than 5% worsening in the model figure of merit. All collected XRR data and the corresponding model fits are given in **SI Figure 4**. See Supporting Information for all calculations.

5. Acknowledgements

Funding: C.B.C. and J.A.V. gratefully acknowledge funding from the Winston Churchill Foundation of the United States. S.F.O. acknowledges financial support from MINECO (CTQ2014-52331R) and Gobierno de Aragón-FEDER-Fondo Social Europeo 2014–2020 (E14_17R). X.Z. acknowledges support from Hong Kong Research Grants Council (HKBU 22304115-ECS and C5015-15GF), Areas of Excellence Scheme ([AoE/P-03/08]) and the Hong Kong Baptist University (RC-ICRS/15-16/02E, RC-ICRS/1617/02C-CHE and RC-IRMS/16/17/02CHEM). J.M.C. thanks the 1851 Royal Commission of the Great Exhibition for the 2014 Fellowship in Design, hosted by Argonne National Laboratory where work was done supported by DOE Office of Science, Office of Basic Energy Sciences, and research resources from the Center of Nanoscale Materials and the Argonne Leadership Computing Facility, which

are DOE Office of Science Facilities, all under contract no. DE-AC02-06CH11357. The authors thank Dr. Erwin Reisner, Department of Chemistry, University of Cambridge for use of laboratory space and equipment. The authors thank the Science and Technology Facilities Council (STFC) for access to facilities at the ISIS Materials Characterisation Laboratory, STFC Rutherford Appleton Laboratory (RAL), and its funding provision for research carried out at the Research Complex at Harwell at RAL. J.M.C. is also indebted to the ISIS Facility at RAL and to Tessella, for financial support (for E.J.B.).

Author Contributions: C.B.C. and J.M.C. conceived and designed the project. E.J.B. and J.M.C. generated the initial database of dyes. C.B.C., J.M.C., and A. V-M. designed and executed the computational workflow. T.T. and K.R.J.T. synthesized dye 8c. J.J. and S.X. synthesized dye XS6. G.B.B., S.C., and X.Z. synthesized dye H3. L.G.A. and S.F.O. synthesized dye 15. A.C. synthesized dye C1. L.S. and J.M.C. fabricated Si wafers with atomic layer deposited TiO_2. C.B.C. performed experimental validation for all of the synthesized dyes. J.A.V. assisted with the photovoltaic measurements and completed NMR measurements. G.B.G.S. and D.W.N. assisted with the AFM and XRR measurements. C.B.C. and J.M.C. wrote the manuscript. All authors edited the manuscript.

Competing Interests: The authors declare that they have no competing interests.

6. References

[1] A. Zunger, *Nat. Rev. Chem.* **2018**, *2*, 0121.
[2] S. Curtarolo, G. L. W. Hart, M. B. Nardelli, N. Mingo, S. Sanvito, O. Levy, *Nat. Mater.* **2013**, *12*, 191.
[3] R. Gautier, X. Zhang, L. Hu, L. Yu, Y. Lin, T. O. L. Sunde, D. Chon, K. R. Poeppelmeier, A. Zunger, *Nat. Chem.* **2015**, *7*, 308.
[4] F. Yan, X. Zhang, Y. G. Yu, L. Yu, A. Nagaraja, T. O. Mason, A. Zunger, *Nat. Commun.* **2015**, *6*, 7308.
[5] A. Zakutayev, X. Zhang, A. Nagaraja, L. Yu, S. Lany, T. O. Mason, D. S. Ginley, A. Zunger, *J. Am. Chem. Soc.* **2013**, *135*, 10048.
[6] L. Yu, A. Zunger, *Phys. Rev. Lett.* **2012**, *108*, 068701.
[7] L.-C. Lin, A. H. Berger, R. L. Martin, J. Kim, J. A. Swisher, K. Jariwala, C. H. Rycroft, A. S. Bhown, M. W. Deem, M. Haranczyk, B. Smit, *Nat. Mater.* **2012**, *11*, 633.
[8] I. E. Castelli, T. Olsen, S. Datta, D. D. Landis, S. Dahl, K. S. Thygesen, K. W. Jacobsen, *Energy Environ. Sci.* **2012**, *5*, 5814.
[9] C. E. Wilmer, M. Leaf, C. Y. Lee, O. K. Farha, B. G. Hauser, J. T. Hupp, R. Q. Snurr, *Nat. Chem.* **2012**, *4*, 83.
[10] A. Peddapuram, H. Cheema, R. E. Adams, R. H. Schmehl, J. H. Delcamp, *J. Phys. Chem. C* **2017**, *121*, 8770.
[11] P. Brogdon, H. Cheema, J. H. Delcamp, *ChemSusChem* **2018**, *11*, 86.
[12] B. E. Hardin, H. J. Snaith, M. D. McGehee, *Nat. Photonics* **2012**, *6*, 162.
[13] M. Freitag, J. Teuscher, Y. Saygili, X. Zhang, F. Giordano, P. Liska, J. Hua, S. M. Zakeeruddin, J.-E. Moser, M. Grätzel, A. Hagfeldt, *Nat. Photonics* **2017**, *11*, 372.
[14] J. Gong, K. Sumathy, Q. Qiao, Z. Zhou, *Renew. Sustain. Energy Rev.* **2017**, *68*, 234.
[15] K. Yoo, J.-Y. Kim, J. A. Lee, J. S. Kim, D.-K. Lee, K. Kim, J. Y. Kim, B. Kim, H. Kim, W. M. Kim, J. H. Kim, M. J. Ko, *ACS Nano* **2015**, *9*, 3760.
[16] Z. Wen, M.-H. Yeh, H. Guo, J. Wang, Y. Zi, W. Xu, J. Deng, L. Zhu, X. Wang, C. Hu, L. Zhu, X. Sun, Z. L. Wang, *Sci. Adv.* **2016**, *2*, DOI 10.1126/sciadv.1600097.
[17] M. J. Yun, S. I. Cha, S. H. Seo, D. Y. Lee, *Sci. Rep.* **2014**, *4*, 5322.
[18] M. Peng, X. Yu, X. Cai, Q. Yang, H. Hu, K. Yan, H. Wang, B. Dong, F. Zhu, D. Zou, *Nano Energy* **2014**, *10*, 117.
[19] H. C. Weerasinghe, F. Huang, Y.-B. Cheng, *Nano Energy* **2013**, *2*, 174.
[20] S. G. Hashmi, M. Özkan, J. Halme, S. M. Zakeeruddin, J. Paltakari, M. Grätzel, P. D. Lund, *Energy Environ. Sci.* **2016**, *9*, 2453.
[21] P. J. Holliman, M. L. Davies, A. Connell, B. V. Velasco, T. M. Watson, *Chem. Commun.* **2010**, *46*, 7256.
[22] P. J. Holliman, M. Mohsen, A. Connell, M. L. Davies, K. Al-Salihi, M. B. Pitak, G. J. Tizzard, S. J. Coles, R. W. Harrington, W. Clegg, C. Serpa, O. H. Fontes, C. Charbonneau, M. J. Carnie, *J. Mater. Chem.* **2012**, *22*, 13318.
[23] K. Kakiage, Y. Aoyama, T. Yano, K. Oya, J. Fujisawa, M. Hanaya, *Chem. Commun.* **2015**, *51*, 15894.
[24] S. L. Bayliss, J. M. Cole, P. G. Waddell, S. McKechnie, X. Liu, *J. Phys. Chem. C* **2014**, *118*, 14082.
[25] F. A. Y. N. Schröder, J. M. Cole, P. G. Waddell, S. McKechnie, *Adv. Energy Mater.* **2015**, *5*, 1401728.

[26] G. Pepe, J. M. Cole, P. G. Waddell, J. R. D. Griffiths, *Mol. Syst. Des. Eng.* **2016**, *1*, 402.
[27] G. Pepe, J. M. Cole, P. G. Waddell, S. McKechnie, *Mol. Syst. Des. Eng.* **2016**, *1*, 86.
[28] M. C. Swain, J. M. Cole, *J. Chem. Inf. Model.* **2016**, *56*, 1894.
[29] L. Zhang, J. M. Cole, *ACS Appl. Mater. Interfaces* **2015**, *7*, 3427.
[30] J. M. Cole, K. S. Low, H. Ozoe, P. Stathi, C. Kitamura, H. Kurata, P. Rudolf, T. Kawase, *Phys. Chem. Chem. Phys.* **2014**, *16*, 26684.
[31] F. Labat, C. Adamo, *J. Phys. Chem. C* **2007**, *111*, 15034.
[32] G. Boschloo, A. Hagfeldt, *Acc. Chem. Res.* **2009**, *42*, 1819.
[33] C. Maglione, A. Carella, R. Centore, S. Fusco, A. Velardo, A. Peluso, D. Colonna, A. Di Carlo, *J. Photochem. Photobiol. Chem.* **2016**, *321*, 79.
[34] D. Karthik, V. Kumar, K. R. Justin Thomas, C.-T. Li, K.-C. Ho, *Dyes Pigments* **2016**, *129*, 60.
[35] L. Zhang, Y. Liu, Z. Wang, M. Liang, Z. Sun, S. Xue, *Tetrahedron* **2010**, *66*, 3318.
[36] R. Pérez-Tejada, N. Martínez de Baroja, S. Franco, L. Pellejà, J. Orduna, R. Andreu, J. Garín, *Dyes Pigments* **2015**, *123*, 293.
[37] Y. Hua, H. Wang, X. Zhu, A. Islam, L. Han, C. Qin, W.-Y. Wong, W.-K. Wong, *Dyes Pigments* **2014**, *102*, 196.
[38] V. Venkatraman, R. Raju, S. P. Oikonomopoulos, B. K. Alsberg, *J. Cheminformatics* **2018**, *10*, 18.
[39] A. B. Nepomnyashchii, B. A. Parkinson, *Langmuir* **2013**, *29*, 9362.
[40] J. McCree-Grey, J. M. Cole, P. J. Evans, *ACS Appl. Mater. Interfaces* **2015**, *7*, 16404.
[41] J. McCree-Grey, J. M. Cole, S. A. Holt, P. J. Evans, Y. Gong, *Nanoscale* **2017**, *9*, 11793.
[42] L. Zhang, J. M. Cole, *J. Mater. Chem. A* **2017**, *5*, 19541.
[43] D. Weininger, *J. Chem. Inf. Comput. Sci.* **1988**, *28*, 31.
[44] D. M. Lowe, P. T. Corbett, P. Murray-Rust, R. C. Glen, *J. Chem. Inf. Model.* **2011**, *51*, 739.
[45] N. M. O'Boyle, M. Banck, C. A. James, C. Morley, T. Vandermeersch, G. R. Hutchison, *J. Cheminformatics* **2011**, *3*, 33.
[46] *RDKit: Open-Source Cheminformatics*, **2017**.
[47] J. Stewart, *MOPAC2016*, Stewart Computational Chemistry, Colorado Springs, CO, USA, **2016**.
[48] R. Ramakrishnan, P. O. Dral, M. Rupp, O. A. von Lilienfeld, *Sci. Data* **2014**, *1*, 140022.
[49] S. A. Rice, M. S. Zhao, *Phys. Rev. B* **1998**, *57*, 13501.
[50] T. Clark, J. Chandrasekhar, G. W. Spitznagel, P. V. R. Schleyer, *J. Comput. Chem.* **1983**, *4*.
[51] A. D. Becke, *J. Chem. Phys.* **1993**, *98*, 5648.
[52] M. Valiev, E. J. Bylaska, N. Govind, K. Kowalski, T. P. Straatsma, H. J. J. Van Dam, D. Wang, J. Nieplocha, E. Apra, T. L. Windus, W. A. de Jong, *Comput. Phys. Commun.* **2010**, *181*, 1477.
[53] D. Nečas, P. Klapetek, *Open Phys.* **2011**, *10*, 181.
[54] M. Björck, G. Andersson, *J. Appl. Crystallogr.* **2007**, *40*, 1174.
[55] F. Schiffmann, J. VandeVondele, J. Hutter, R. Wirz, A. Urakawa, A. Baiker, *J. Phys. Chem. C* **2010**, *114*, 8398.
[56] G. Pepe, J. M. Cole, P. G. Waddell, J. I. Perry, *Mol. Syst. Des. Eng.* **2016**, *1*, 416.

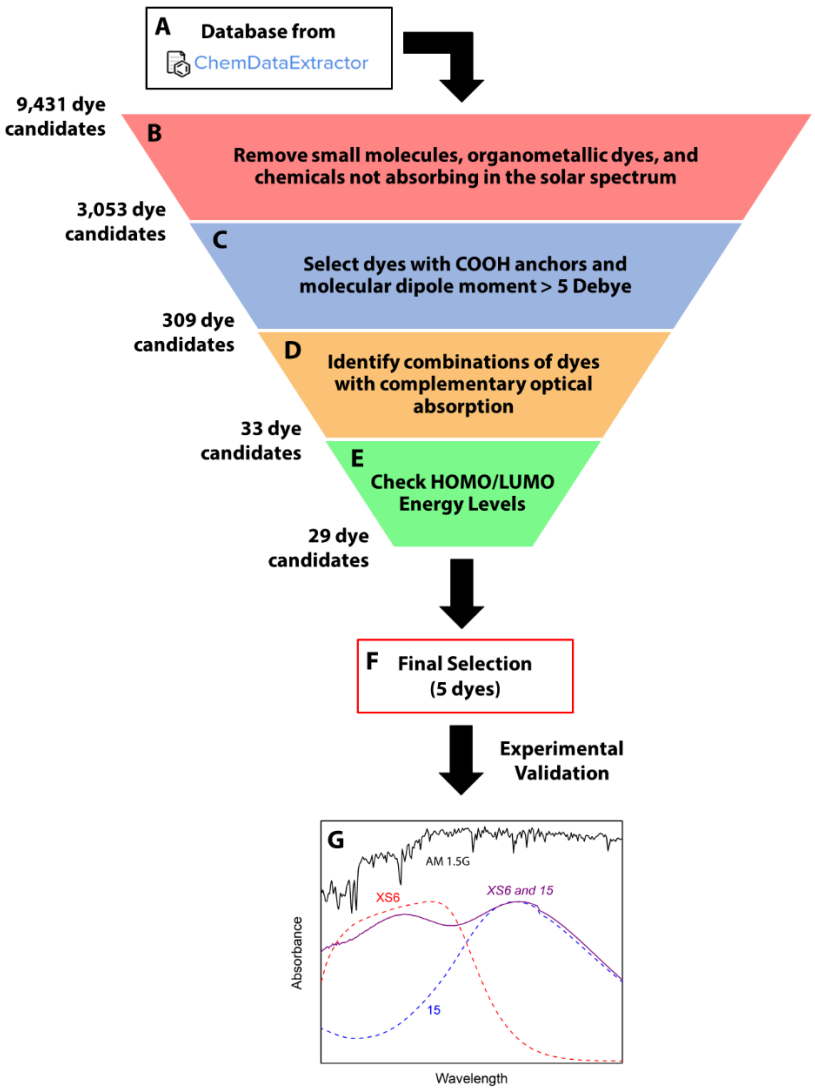

Fig. 1: Design-to-device approach to create panchromatic solar cells via co-sensitization. **A)** A starting database of 9,431 dye candidates from the academic literature is auto-generated using the text-mining tool, ChemDataExtractor. **B)** Initial screens remove small molecules, organometallic dyes, and chemicals not absorbing in the solar spectrum (350 – 1000 nm) to reduce the number of dyes to 3,053. **C)** Substructure searching and semi-empirical calculations are used to select dyes with a carboxylic acid anchor and a molecular dipole moment > 5 Debye. **D)** A novel algorithm predicts optimal combinations of dyes with complementary optical absorption spectra and high molar extinction coefficients, narrowing the shortlist to 33 dyes. **E)** The highest-occupied molecular orbital (HOMO) and lowest-unoccupied molecular orbital (LUMO) energy levels of each dye are checked using density functional theory (DFT) to ensure proper integration into a DSSC. **F)** A final set of five dyes is selected for experimental verification based on practical constraints such as ease of synthesis and availability. **G)** Experimental validation illustrates the benefits of co-sensitization and shows how the best performing combination of two dyes with complementary optical absorption spectra, XS6 (red) and 15 (blue), affords a co-sensitized DSSC, *XS6 and 15* (purple), with broad absorbance. The AM 1.5G solar emission spectrum (black) is offset above for reference.

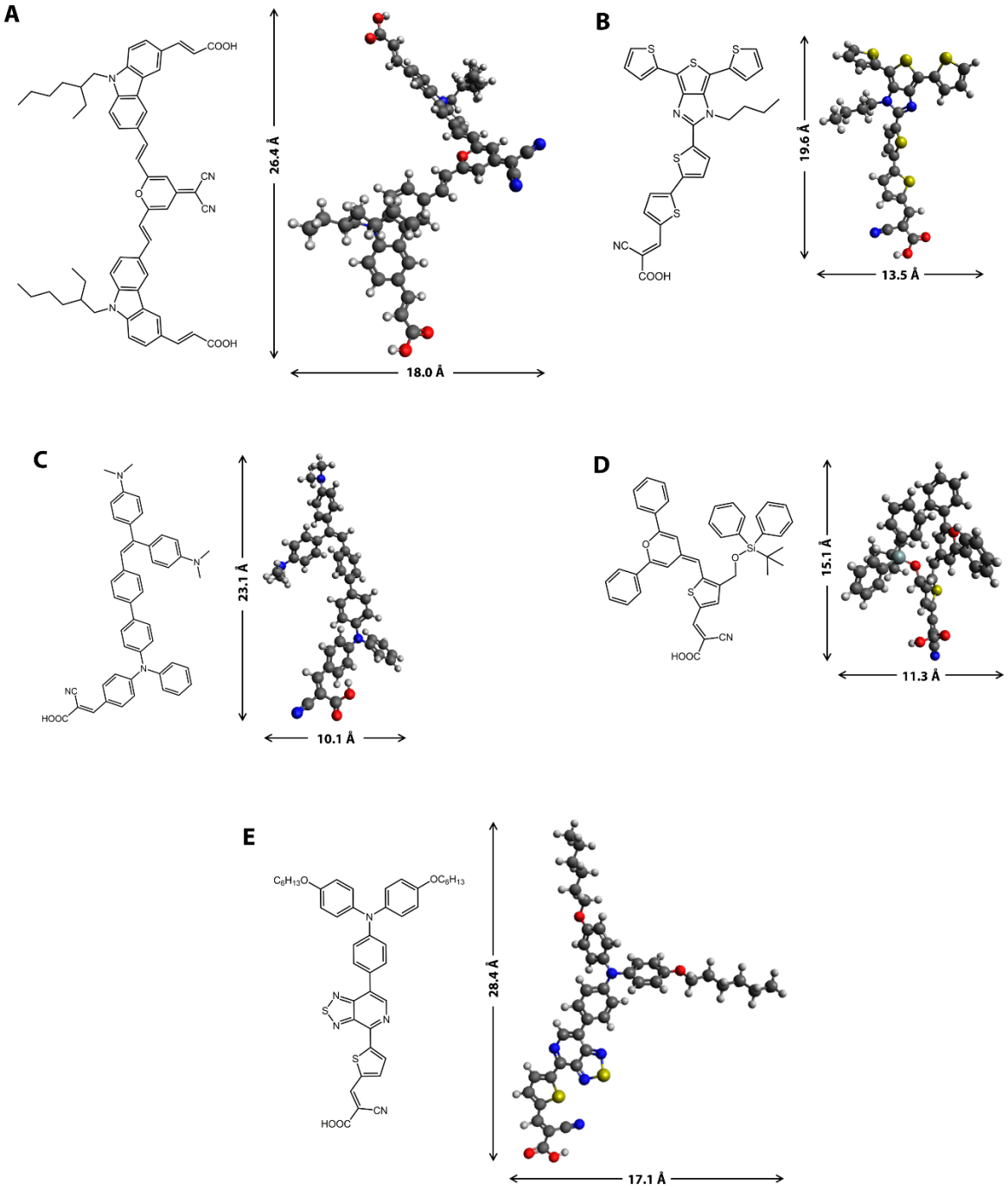

Fig. 2: Chemical structures of predicted dyes.
The 2D and 3D chemical structures of dyes C1 (**A**), 8c (**B**), XS6 (**C**), 15 (**D**), and H3 (**E**) with annotated molecular length and width marked for each dye. Molecular length is defined as the largest atom-to-atom distance projected from either oxygen in the carboxylate anchor of each dye. The molecular width is defined as the largest atom-to-atom distance perpendicular to the molecular length. 3D structures are optimized with PM7 semi-empirical calculations.

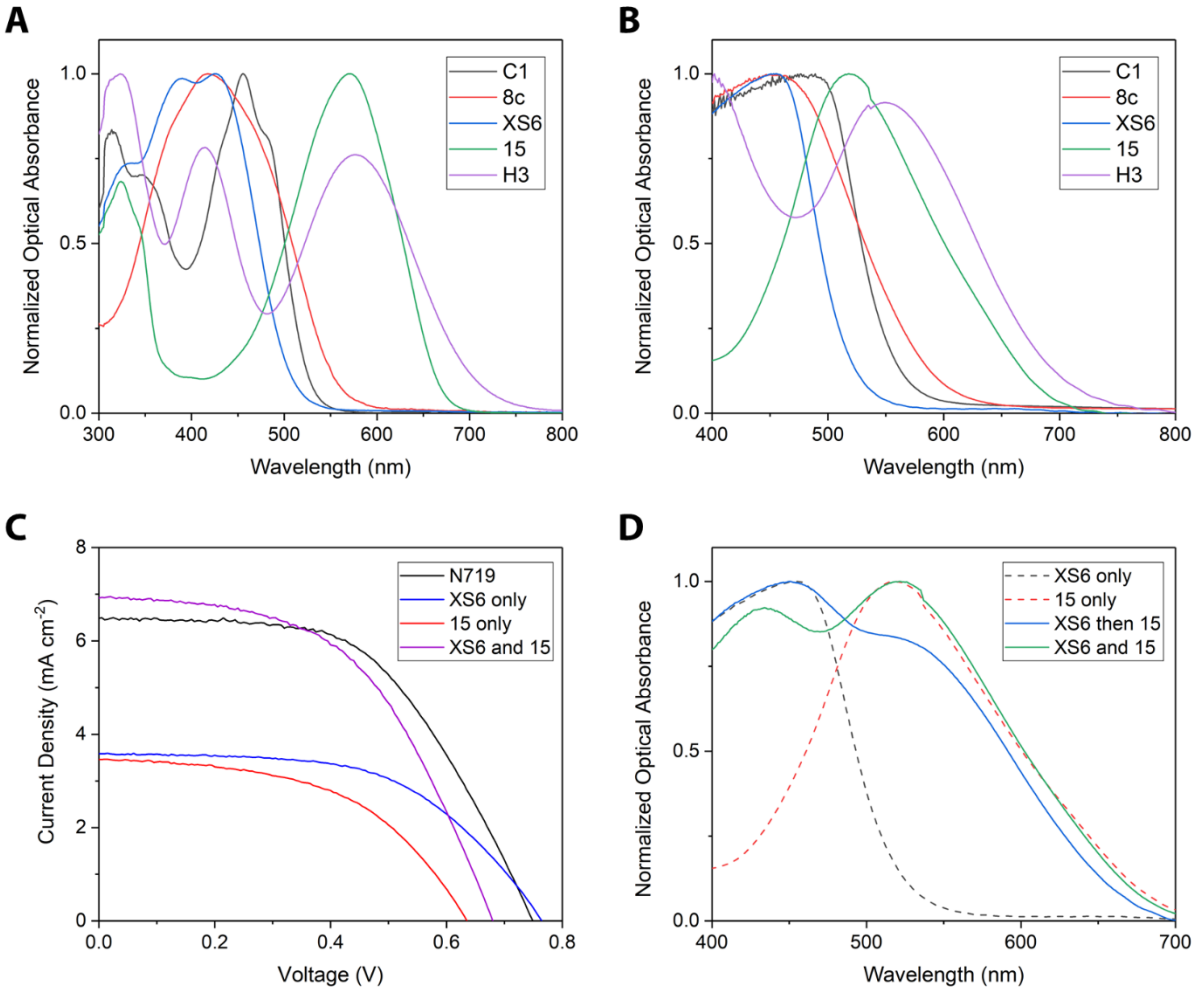

Fig. 3: Optical absorption and photovoltaic performance.
Optical absorption of the predicted dyes in DCM solution (**A**) and adsorbed onto TiO_2 (**B**). **C**) J-V curves of DSSCs sensitized with XS6 only (blue), 15 only (red), and both XS6 and 15 (purple) compared to an N719 reference (black). The *XS6 and 15* co-sensitized DSSC demonstrates dramatic improvements compared to the singly-sensitized DSSC with performance comparable to the N719 reference. **D)** Optical absorption of co-sensitized WEs *XS6 then 15* and *XS6 and 15* compared to their XS6 and 15 singly-sensitized counterparts. Both co-sensitized WEs exhibit broad absorbance compared to the singly-sensitized WEs, with that of *XS6 and 15* having a higher concentration ratio of 15:XS6 adsorbed to the TiO_2 surface as indicated by the shift in maximum absorbance.

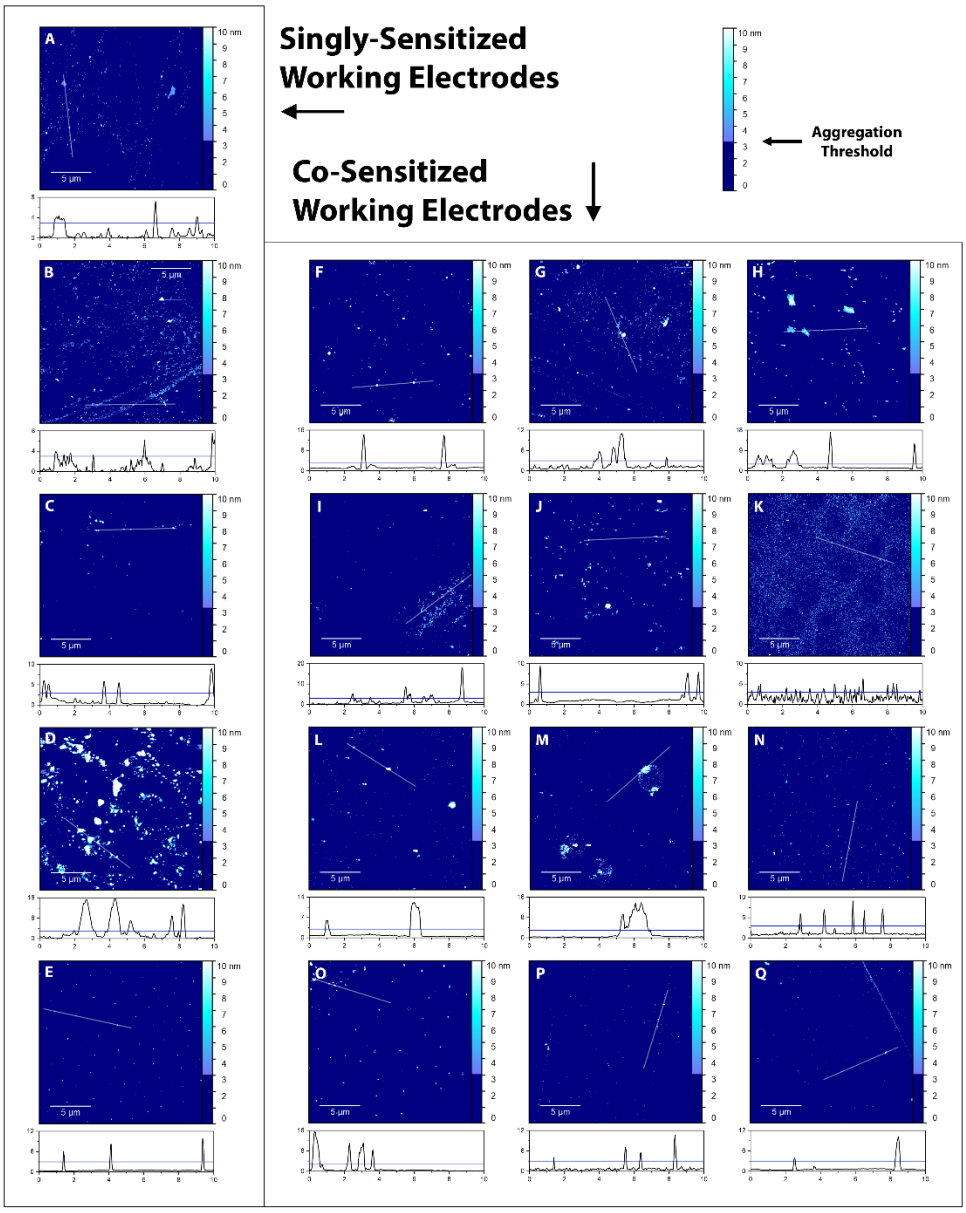

Fig. 4: Surface characterization via AFM.
Representative 20 x 20 µm AFM images for dyes C1 (**A**), 8c (**B**), XS6 (**C**), 15 (**D**), and H3 (**E**). Representative 20 x 20 µm AFM images for dye combinations C1 then 15 (**F**), C1 and 15 (**G**), H3 then C1 (**H**), C1 and H3 (**I**), 8c then 15 (**J**), 8c and 15 (**K**), H3 then 8c (**L**) , 8c and H3 (**M**), XS6 then 15 (**N**), XS6 and 15 (**O**), XS6 then H3 (**P**), and XS6 and H3 (**Q**). The color bar is solid below the 3 nm aggregation threshold. Below each AFM image is a randomly-selected height profile (black) that corresponds to the surface features highlighted by the white trace on the AFM image (from left to right). A blue line showing the aggregation threshold of 3 nm is also included as a visual aid to see features included in the data analysis. Units on the abscissa and ordinate of the height profile are µm and nm, respectively. All AFM images are provided in the Supporting Information.

Table 1. Surface Characterization of Singly-sensitized and Co-sensitized Working Electrodes

Sample Name	AFM Parameters				XRR Parameters			
	Mean Height (nm)	**Max Height (nm)**	**Aggregate Coverage (%)**	**Number of Aggregates (per μm^2)**	**Dye Layer Thickness (Å)**	**SLD$_{dye}$ (x 10^{-6} Å^{-2})**	**Surface Roughness (Å)**	**Surface Coverage (%)**
Singly-sensitized Working Electrodes								
C1 only	5 ± 1	7 ± 2	3 ± 6	2 ± 3	43.5 ± 0.9	6.6 ± 0.5	5.6 ± 0.7	55 ± 4
8c only	5 ± 1	6 ± 2	3 ± 2	3 ± 2	26.6 ± 0.9	5.1 ± 0.9	3.3 ± 0.8	39 ± 7
XS6 only	4.9 ± 0.4	6.0 ± 0.7	1.0 ± 0.1	0.3 ± 0.2	23.6 ± 0.5	8.7 ± 0.4	3.7 ± 0.5	73 ± 3
H3 only	9 ± 1	15 ± 3	0.3 ± 0.1	0.18 ± 0.05	27 ± 1	6.7 ± 0.5	3.7 ± 0.5	55 ± 4
15 only	8 ± 2	15 ± 3	7 ± 2	1.1 ± 0.4	24.3 ± 0.3	7.8 ± 0.4	2.7 ± 0.3	62 ± 3
Co-Sensitized Working Electrodes								
C1 then 15	6 ± 2	10 ± 3	1.3 ± 0.5	0.7 ± 0.2	33.7 ± 0.5	5.9 ± 0.7	3.1 ± 0.6	49 ± 6
C1 and 15	7 ± 2	12 ± 4	2.0 ± 0.5	0.9 ± 0.6	21.5 ± 0.8	6.3 ± 0.9	3.8 ± 0.7	52 ± 7
H3 then C1	8 ± 2	16 ± 4	3 ± 3	0.4 ± 0.2	42 ± 1	6.0 ± 0.6	5.2 ± 0.7	49 ± 5
C1 and H3	5 ± 1	8 ± 3	2 ± 1	2 ± 2	25.4 ± 0.4	8.5 ± 0.4	3.0 ± 0.5	69 ± 3
8c then 15	6 ± 1	9 ± 2	1.1 ± 0.2	0.7 ± 0.6	30.9 ± 0.4	6.9 ± 0.4	3.9 ± 0.6	54 ± 3
8c and 15	4.6 ± 0.3	5.8 ± 0.4	12 ± 9	16 ± 5	31 ± 2	5.7 ± 0.5	7 ± 2	45 ± 4
H3 then 8c	5.5 ± 0.7	8 ± 1	3 ± 2	1 ± 1	37.2 ± 0.2	9.0 ± 0.7	2.9 ± 0.4	70 ± 5
8c and H3	5.2 ± 0.7	7 ± 2	2 ± 2	1 ± 1	27.5 ± 0.4	8.0 ± 0.4	3.3 ± 0.6	63 ± 3
XS6 then 15	**6 ± 1**	**8 ± 2**	**0.7 ± 0.3**	**0.8 ± 0.3**	**18.8 ± 0.3**	**8.7 ± 0.5**	**3.6 ± 0.4**	**72 ± 4**
XS6 and 15	**7.8 ± 0.7**	**11 ± 1**	**0.3 ± 0.1**	**0.24 ± 0.09**	**18.6 ± 0.3**	**8.8 ± 0.5**	**3.4 ± 0.4**	**73 ± 4**
XS6 then H3	5.5 ± 0.7	7.6 ± 0.8	0.3 ± 0.1	0.25 ± 0.04	21.0 ± 0.3	9.6 ± 0.5	4.1 ± 0.4	79 ± 4
XS6 and H3	5.3 ± 0.8	7 ± 1	0.3 ± 0.1	0.2 ± 0.1	21.6 ± 0.6	8.7 ± 0.6	4.0 ± 0.5	71 ± 5

Supporting Information for
"Design-to-Device Approach Affords Panchromatic Co-sensitized Solar Cells"

SI Note 1. Dye Matching Algorithm

A novel algorithm was employed to predict optimal combinations of two, three, or four dyes for co-sensitization. Using the known optical absorption peak wavelength, λ_{max}, and extinction coefficients, ε, of individual dyes that were auto-extracted from the literature, we estimated the fraction of photons absorbed for each wavelength for each dye as a function, $d_i(\lambda)$. This function was generated by treating each known optical absorption peak as a triangular peak with a fixed width and a height weighted by the molar extinction coefficient of the peak. For each dye, the resulting $d_i(\lambda)$ represents the predicted absorbance of the dye at each wavelength as normalized within a range from 0 to 1. This function is referred to as the proxy spectrum of the dye since it serves as a proxy for the actual (but not known) optical absorption spectral profile of the dye.

For a given combination of n dyes, a combined proxy spectrum of $c(\lambda)$ was calculated as follows:

$$c(\lambda) = \sum_{i=1}^{n} d_i(\lambda) \tag{S1}$$

subject to the constraint that $c(\lambda)$ can never be greater than 1. **SI Fig. 6** gives an example of two dyes with proxy spectra $d_1(\lambda)$ and $d_2(\lambda)$, which are then combined to form the co-sensitized proxy spectra $c(\lambda)$. $d_1(\lambda)$ has a higher extinction coefficient (and thus higher proxy absorbance at its peak) than $d_2(\lambda)$; however, $d_2(\lambda)$ has an optical absorption peak at a higher wavelength than $d_1(\lambda)$ making the two dyes good candidates for co-sensitization.

We ranked each dye combination relative to other possible combinations via a quality factor that consisted of three components: the overlap factor, the absorption fraction, and the relative change. The overlap factor (σ) measures the extent to which the proxy spectra of any two dyes in the co-sensitization overlap (i.e. absorb at the same wavelengths) and ranges from 0 (complete overlap) to 1 (no overlap). Thus, it can be calculated:

$$\sigma = \frac{\int |d_i(\lambda) - d_j(\lambda)|\, d\lambda}{\int d_i(\lambda)\, d\lambda + \int d_j(\lambda) d\lambda} \tag{S2}$$

For combinations of three or more dyes, the overall overlap was calculated by multiplying the overlap factors of each possible pair of dyes within the combination. This ensures that none of the dyes in a given combination overlap significantly with each other.

Using the combined proxy spectra, $c(\lambda)$, the absorption fraction (α) was found by the following equation:

$$\alpha = \frac{\int c(\lambda) * s(\lambda)\, d\lambda}{\int s(\lambda)\, d\lambda} \tag{S3}$$

where $s(\lambda)$ is a polynomial regression that represents the number of photons emitted by AM 1.5 sunlight at each wavelength. Thus, the absorption fraction quantifies the extent to which a given dye combination absorbs the light emitted by the sun, ranging from 0 (no sunlight absorbed) to 1 (all sunlight absorbed).

Finally, the relative change (ω) measures the variation in the absorption fraction caused by the most recent dye addition relative to the maximum possible change (i.e. reaching an absorption fraction of 1). This quantifies the extent to which the tested co-sensitization increases the number of photons absorbed, ranging from 0 (no improvement) to 1 (maximum improvement) and can be calculated by:

$$\omega = \frac{\alpha - \alpha_{max}}{1 - \alpha_{max}} \quad \text{(S4)}$$

where α is the absorption fraction of the combination of n dyes and α_{max} is the maximum absorption fraction of $n - 1$ dyes of the n dyes used in the co-sensitization.

The quality factor was then given by:

$$q = \sigma * \alpha * \omega \quad \text{(S5)}$$

where q ranges from 0 to 1, with 1 being the most ideal co-sensitization. Since considering all combinations of dyes is an increasingly complex combinatorial problem, we screened dye combinations using the overlap factor, skipping all dye combinations in which a pair of dyes had an overlap factor > 0.8. Thus, the algorithm evaluated the quality score of each dye combination, skipping those with low overlap factors, and then ranked the combinations based on their assigned quality score. Selecting the top ten dye pairs and triples and the top five dye quadruples and removing duplicates produced a shortlist of 33 dyes.

SI Note 2. DSSC Fabrication

Working Electrode for UV-Vis Absorption Spectroscopy

Transparent fluorine-doped tin oxide (FTO) glass (TEC 15, Dyesol) with a thickness of 2.2 mm was cut into 30 mm x 50 mm sheets. The sheets were cleaned by sonicating them for 15 minutes in a solution of 5% Decon 90 in deionized (DI) water by volume, then again in DI water, and lastly in ethanol. The glass was then dried with a flow of nitrogen. A layer of TiO_2 nanoparticles was added on top of the FTO glass using TiO_2 paste (Dyesol, DSL 18 NR-T). After taping the edges of the glass (Scotch Magic Tape, 3M), the TiO_2 paste was spread over the exposed FTO glass surface using the doctor-blade method to create a TiO2 layer with an approximate thickness of 5-6 μm. The tape was removed, and the sample was heated gradually in an oven at 8°C per minute to 500°C, held for 30 minutes, and then allowed to cool slowly to room temperature. The sample was then cut into 10 pieces (15 mm x 10 mm). For each dye or set of dyes, a 0.3 mM dye solution was prepared in dichloromethane (DCM). The FTO glass was immersed into the prepared dye solution for ~24 hours (TiO_2 layer facing up). The electrode was then removed from the solution, washed with DCM to remove any non-adsorbed dye on the surface, and dried with a flow of nitrogen.

Working Electrode for X-Ray Reflectometry and Atomic Force Microscopy

A silicon wafer with a 5 nm thick layer of TiO_2 was fabricated by atomic layer deposition at the Center of Nanoscale Materials, Argonne National Laboratory, USA, and cut into 10 mm x 10 mm sheets. For each dye or set of dyes, a 0.3 mM dye solution was prepared in DCM. The silicon wafer substrate was immersed into the prepared dye solution for ~24 hours (TiO_2 layer

facing up). The WE was then removed from the solution, washed with DCM to remove any non-adsorbed dye on the surface, and dried with a flow of nitrogen.

Fabrication of DSSC for Photovoltaic Testing

WEs of the DSSCs featuring the subject dyes were fabricated using the method above. WEs sensitized with the reference dye N719, were fabricated using 0.3 mM dye solution composed of a 1:1 mixture of tert-butanol and acetonitrile instead of DCM. The device area of 0.30 cm^2 for each working electrode was determined by manually removing the TiO2 layer by scraping. The counter electrode for all DSSCs was fabricated by first cutting transparent fluorine-doped tin oxide (FTO) glass (TEC 15, Dyesol) with a thickness of 2.2 mm into 30 mm x 60 mm sheets. The sheets were cleaned by sonicating them for 15 minutes in a solution of 5% Decon 90 in deionized (DI) water by volume, then again in DI water, and lastly in ethanol. The glass was then dried with a flow of nitrogen. A layer of Pt nanoparticles was added on top of the FTO glass using Pt paste (Platisol, Solaronix). After taping the edges of the glass, the Pt paste was spread over the exposed FTO glass surface using the doctor-blade method. The tape was removed, and the sample was heated gradually in an oven at 8°C per minute to 450°C, held for 30 minutes, and then allowed to cool slowly to room temperature. The sample was then cut into 10 pieces (15 mm x 20 mm). Operational DSSCs were fabricated by mechanically sealing the working and counter electrodes with a paraffin gasket (Parafilm) and electrolyte (EL-HPE, Sigma) containing acetonitrile, valeronitrile, 1-Butyl-3-mthylimidazolium iodide, 4-tert-Butylpyridine, Guanidinium thiocyanate, and iodine.

SI Note 3. XRR Analysis

Reflectivity was plotted against the momentum transfer vector (Q) found by:

$$Q = \frac{4\pi sin(\phi)}{\lambda} \tag{S6}$$

where ϕ and λ are the angle and wavelength of the incident light, respectively.

The SLD of each individual dye was approximated by[40]:

$$SLD_{ideal} = \frac{r_e Z}{V} \tag{S7}$$

where r_e is the classical electron radius (2.81 x 10^{-5} Å), Z is the total number of electrons in the dye, and V is the molecular volume, estimated by PM7 semi-empirical calculations. The calculated SLD values for each dye are given in **SI Table 3** along with the chemical formula, total number of electrons, volume, and molecular dimensions (length, l, and width, w) as defined in **Figure 2**. Eqns. S8-12 are based on previous work on the XRR analysis of DSSCs.[40,41]

The surface coverage for each sample was calculated as:

$$x = \frac{SLD_{measured}}{SLD_{ideal}} \tag{S8}$$

where $x = 0$ indicates no coverage and $x = 1$ indicates complete coverage of the TiO_2 surface. For a singly-sensitized WE, SLD_{ideal} equals the approximated SLD of the dye reported in **SI**

Table 3. For co-sensitized WEs, we estimate SLD_{ideal} as the average SLD value for the two sensitized dyes, which is appropriate given the high similarity between SLD values for all the dyes (within 10%).

For an adsorbed dye monolayer (i.e. when the dye-layer thickness is not greater than the molecular length of the dye), the average measured area per dye molecule (APM) in the monolayer can be found by:

$$APM = \frac{V}{xd} \tag{S9}$$

where V is the molecular volume of the dye and d is the fitted dye-layer thickness. The APM can then be used to calculate the surface concentration of the dye ($[dye]_{surf}$) and the average intermolecular spacing between each dye (δ) via the following equations.

$$[dye]_{surf} = \frac{1}{N_A * APM} \tag{S10}$$

$$\delta = \frac{APM}{w} \tag{S11}$$

where N_A is Avogadro's constant and w is the calculated molecular width of the dye. Lastly, the maximum possible dye-layer thickness (d_{max}) is the sum of the molecular length of the dye and the average dye···TiO_2 separation for a carboxylate···TiO_2 bond (2.05 Å).[55] The adsorption tilt angle (θ) (i.e. the angle that the dye makes with the TiO_2 surface when adsorbed) can then be found by:

$$\sin(\theta) = \frac{d}{d_{max}} \tag{S12}$$

Using these equations allows one to determine that dyes XS6 and H3 had calculated surface concentrations of $3.4 \pm 0.2 \times 10^{-10}$ and $2.8 \pm 0.2 \times 10^{-10}$ mol cm^{-2}, average intermolecular spacings of 3.7 ± 0.2 and 2.8 ± 0.1 Å, and adsorption tilt angles of 70 ± 2 and $53.0 \pm 0.7°$, respectively.

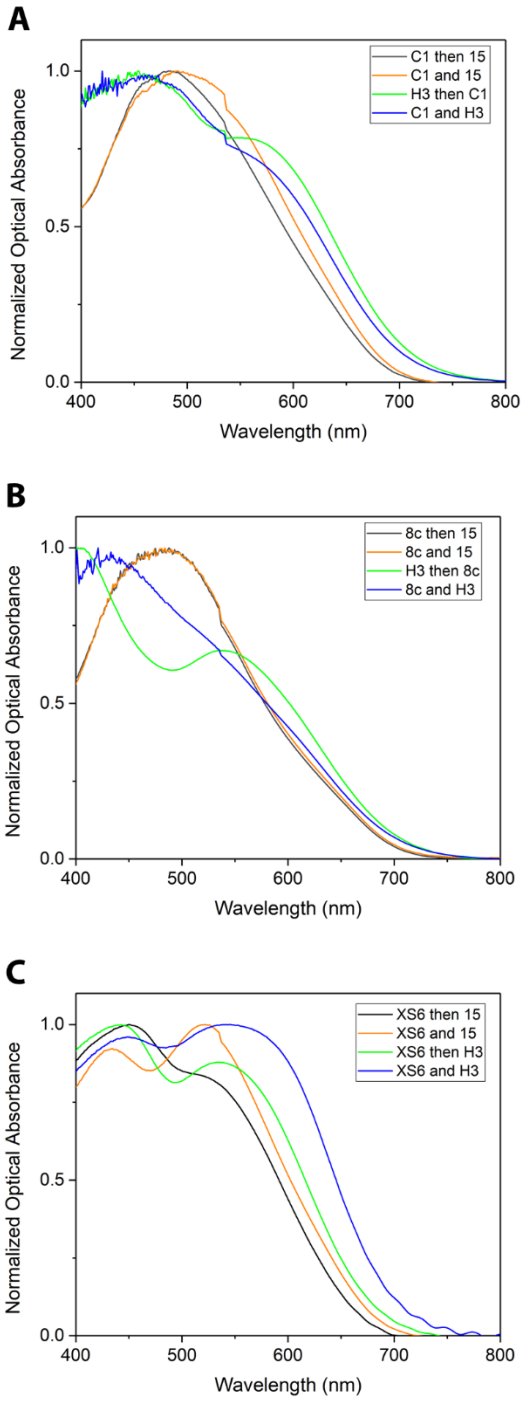

SI Fig. 1. Optical absorption spectra of co-sensitized working electrodes fabricated by various sensitization methods for each pair of dyes: **(A)** C1 with 15 and C1 with H3, **(B)** 8c with 15 and 8c with H3, **(C)** XS6 with 15 and XS6 with H3.

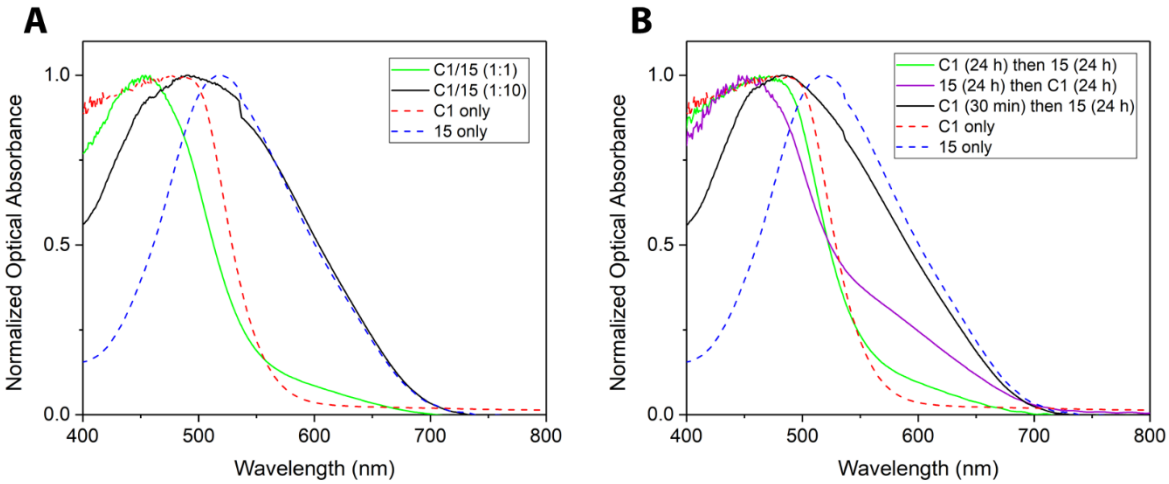

SI Fig. 2. Optical absorption spectra acquired on working electrodes co-sensitized with dyes C1 and 15 under various experimental conditions to show how C1 can desorb 15. **(A)** Co-sensitized working electrodes sensitized via the cocktail method compared to singly-sensitized working electrodes. **(B)** Co-sensitized working electrodes sensitized via the sequential method while compared to singly-sensitized working electrodes.

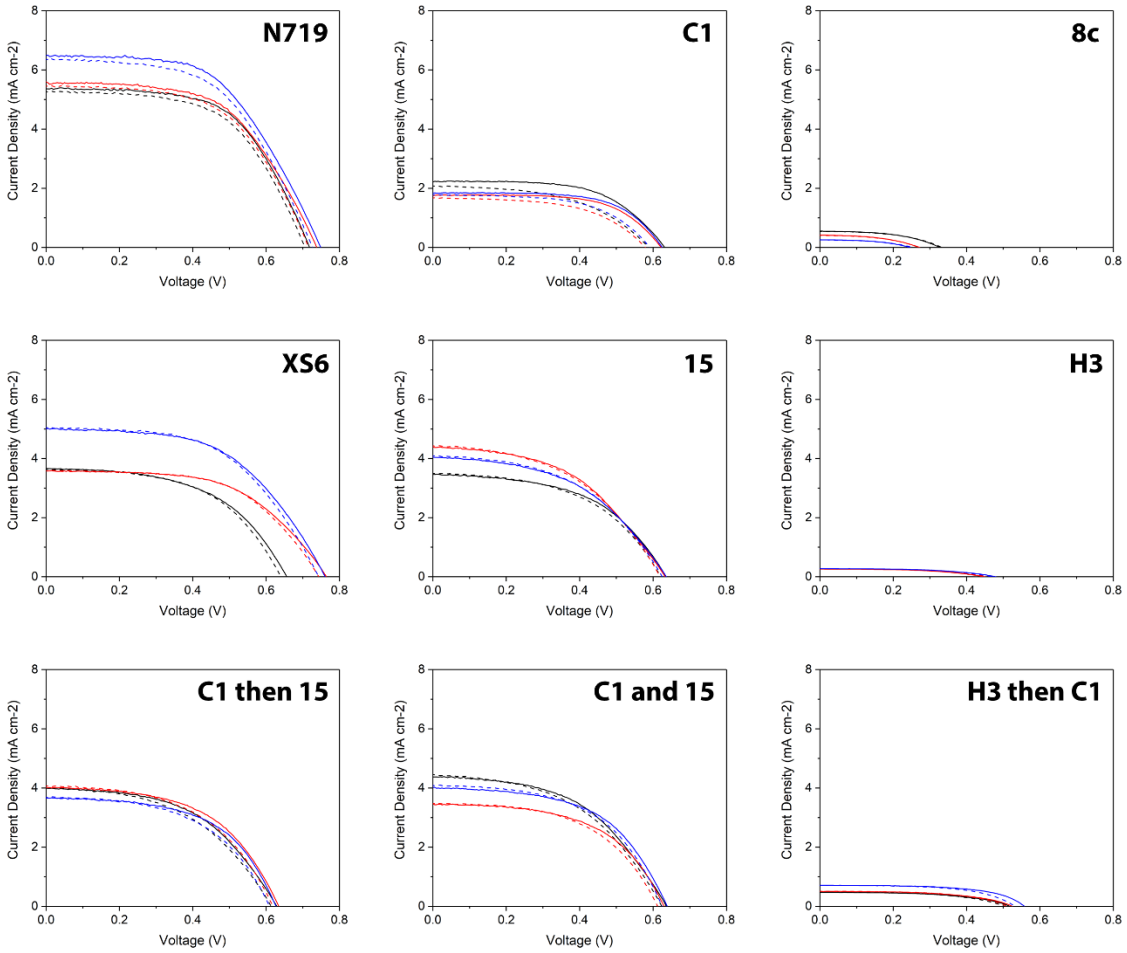

SI Fig. 3. J-V curves for all working electrodes (continued on next page). The forward and backward J-V traces are given as solid and dashed lines, respectively. Photovoltaic measurements for three independent DSSCs are given as red, blue, and black lines. It is the relative comparisons that are meaningful (see note on SI Table 2).

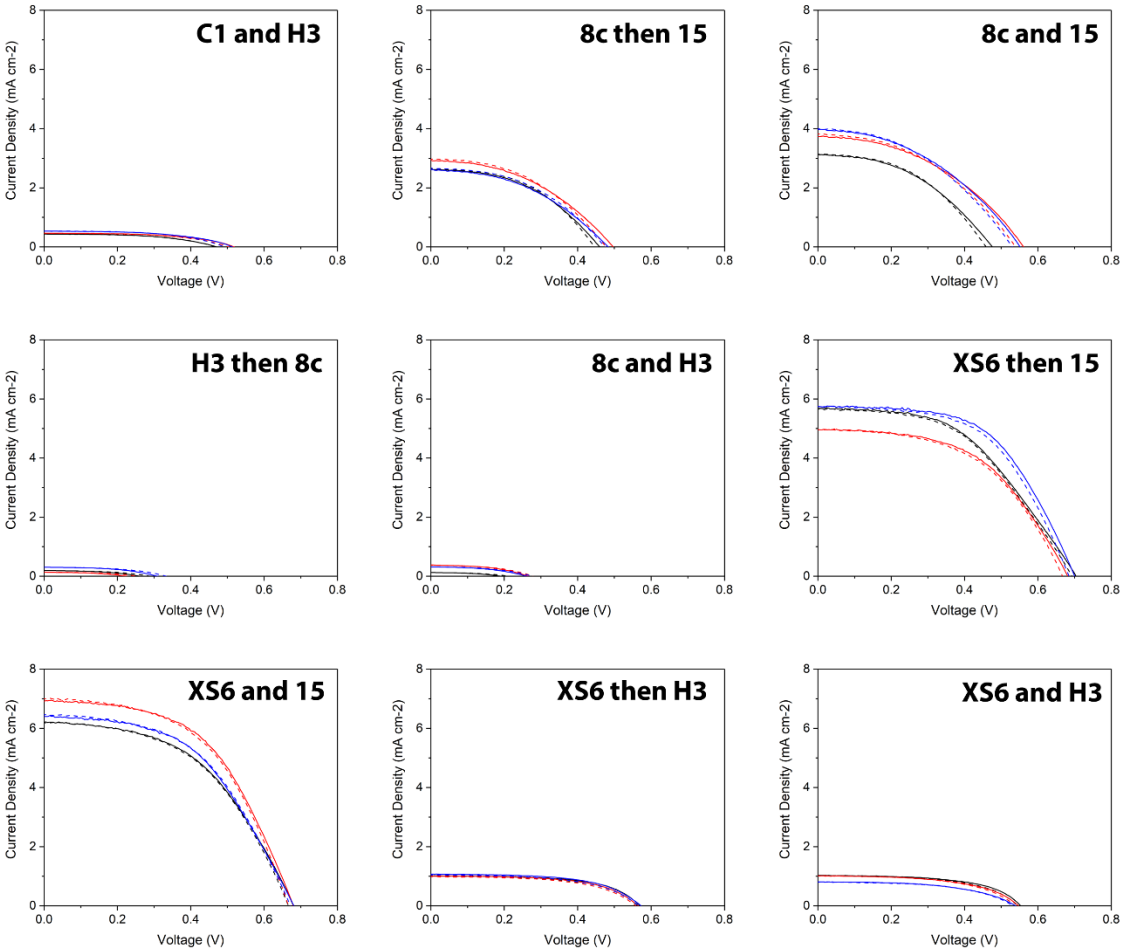
C1 and H3
8c then 15
8c and 15
H3 then 8c
8c and H3
XS6 then 15
XS6 and 15
XS6 then H3
XS6 and H3
Current Density (mA cm-2)
Voltage (V)

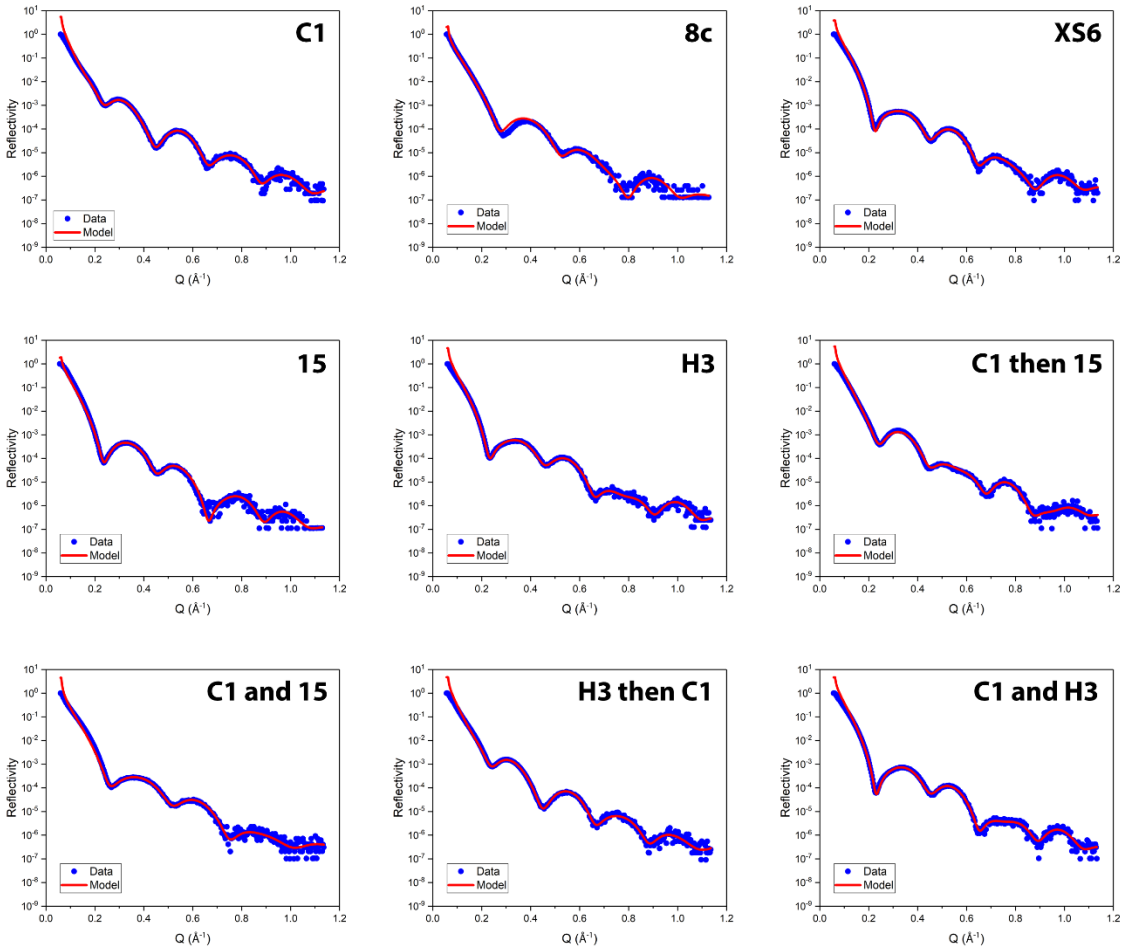

SI Fig. 4. XRR data (blue dots) and the fitted model (black line) for all working electrodes

(continued on next page).

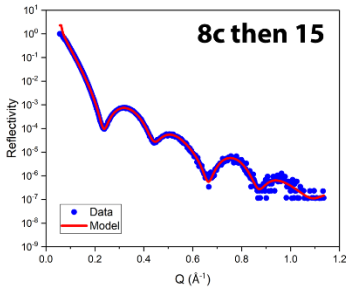
8c then 15
Reflectivity
Q (Å^{-1})
Data
Model

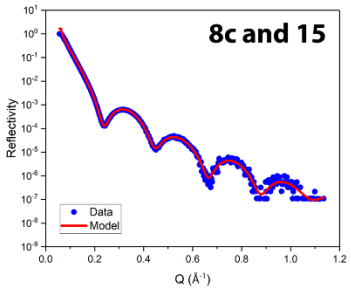
8c and 15
Reflectivity
Q (Å^{-1})
Data
Model

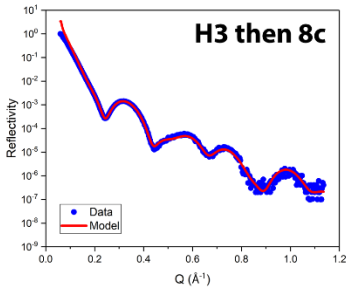
H3 then 8c
Reflectivity
Q (Å^{-1})
Data
Model

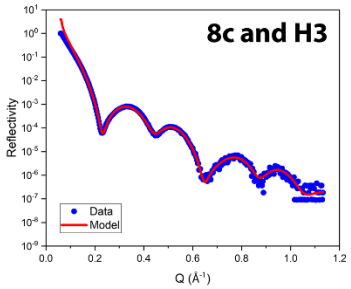
8c and H3
Reflectivity
Q (Å^{-1})
Data
Model

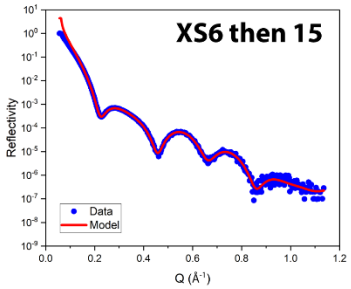
XS6 then 15
Reflectivity
Q (Å^{-1})
Data
Model

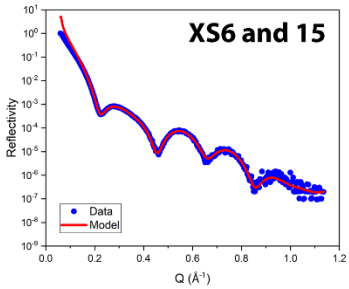
XS6 and 15
Reflectivity
Q (Å^{-1})
Data
Model

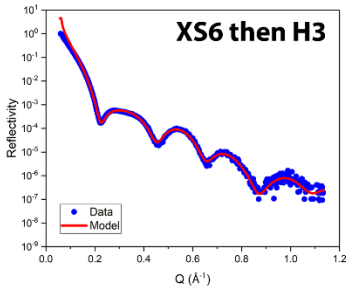
XS6 then H3
Reflectivity
Q (Å^{-1})
Data
Model

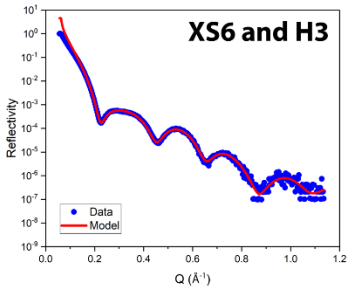
XS6 and H3
Reflectivity
Q (Å^{-1})
Data
Model

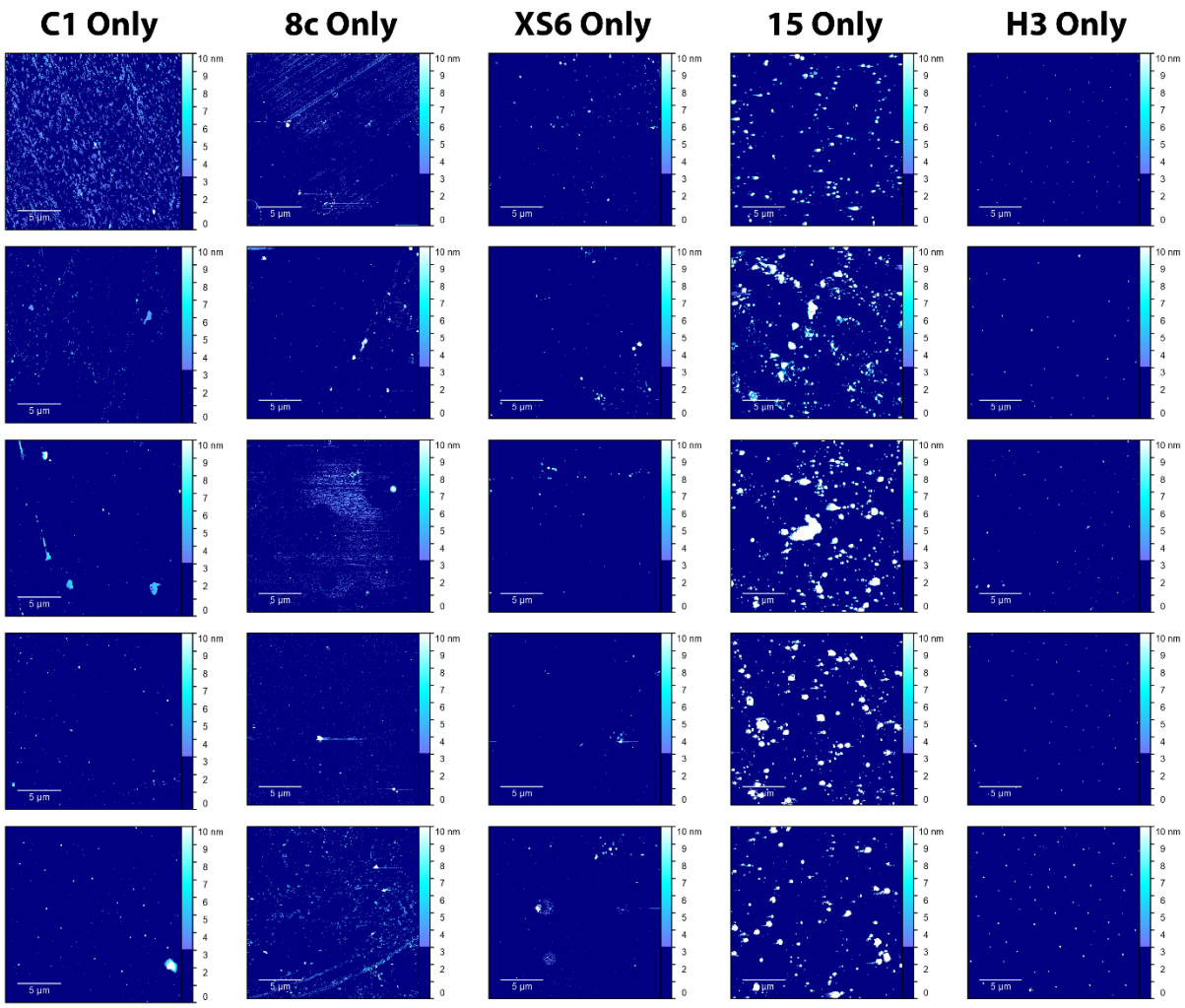

SI Fig. 5. The AFM images (five per WE) used for the quantitative analysis of dye aggregation in the DSSCs (continued on the next pages). The aggregation threshold of 3 nm is shown on the color bar.

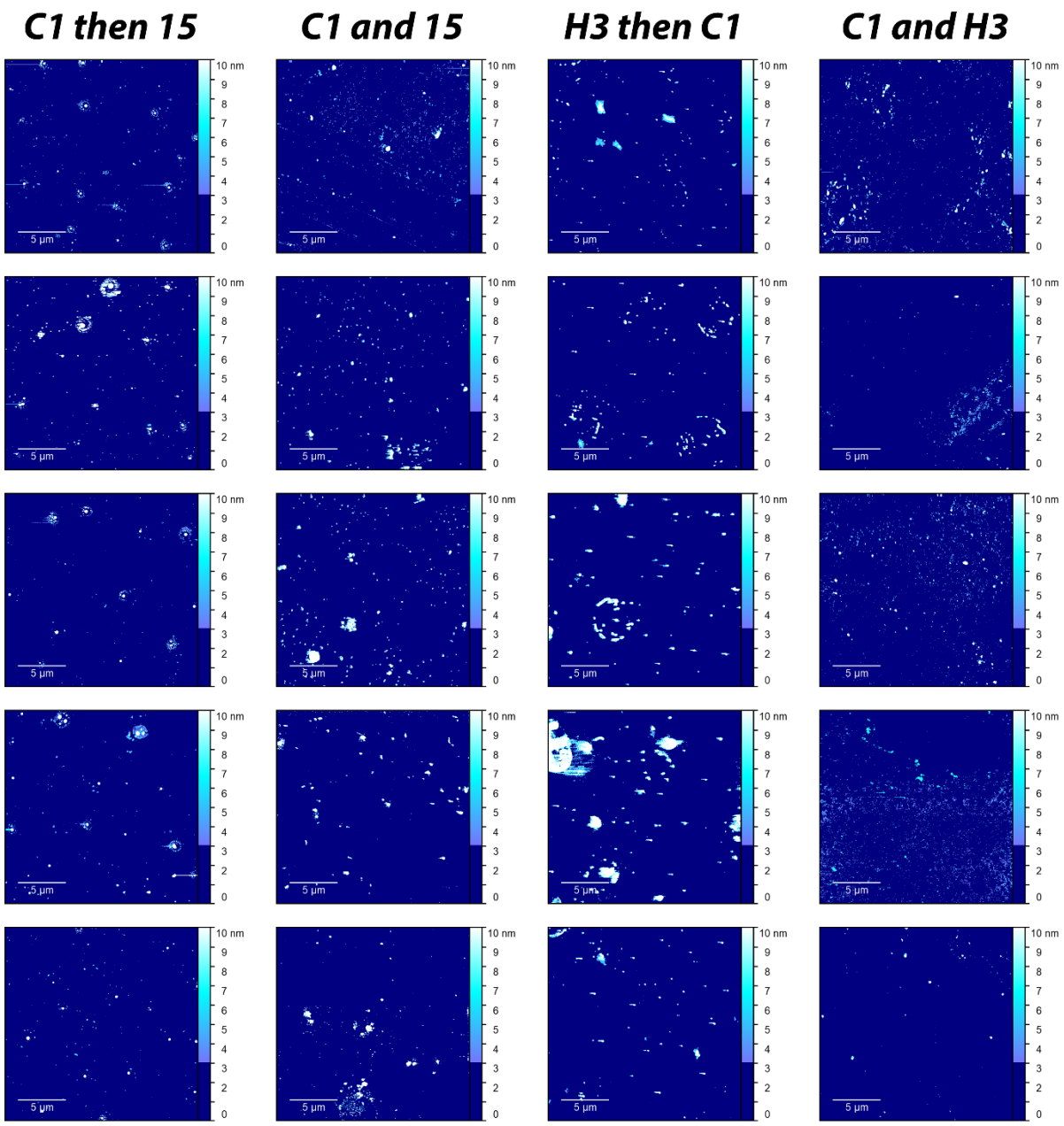
C1 then 15
C1 and 15
H3 then C1
C1 and H3
10 nm
9
8
7
6
5
4
3
2
0
5 µm

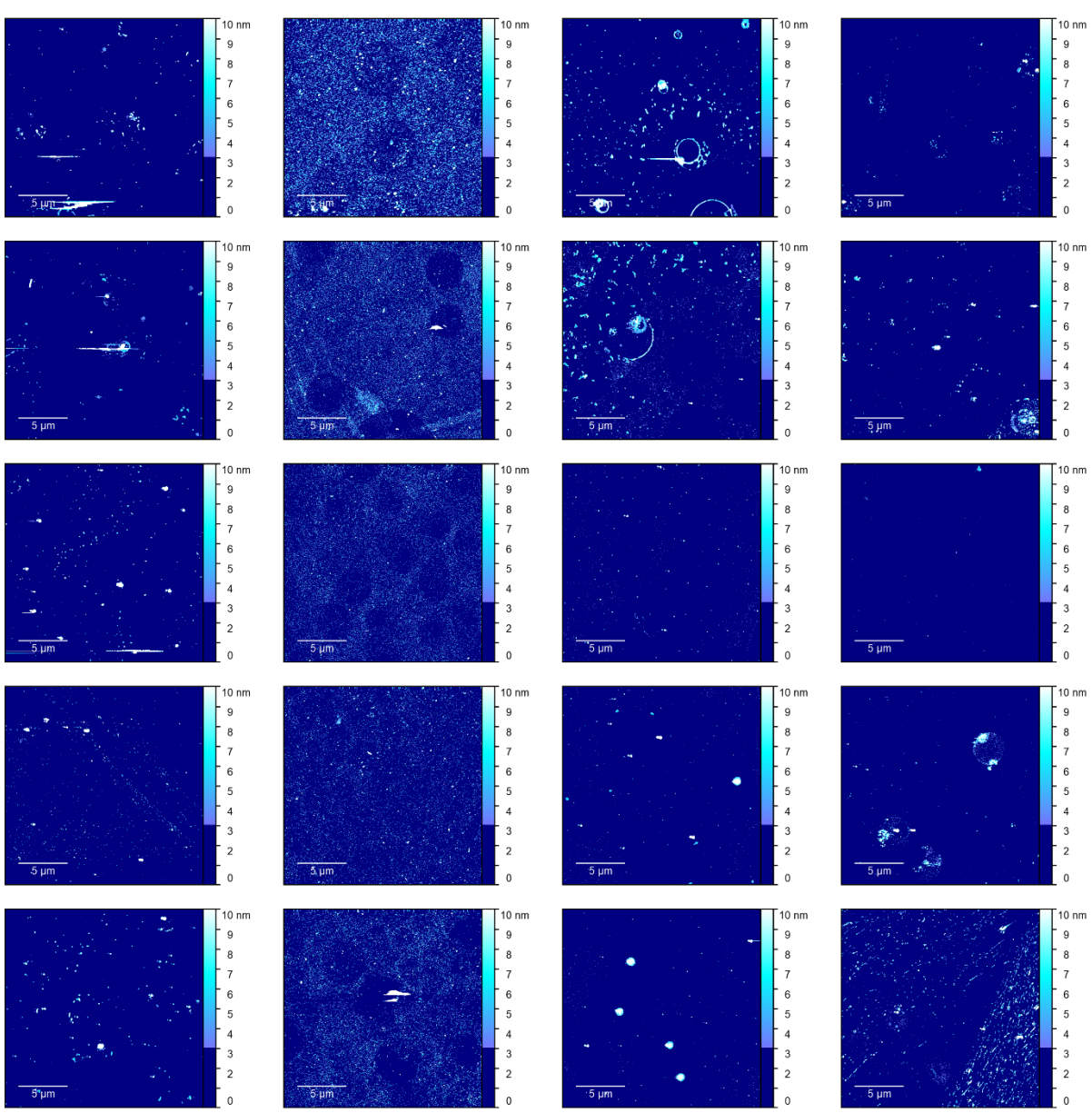
8c then 15
8c and 15
H3 then 8c
8c and H3
10 nm
9
8
7
6
5
4
3
2
0
5 µm

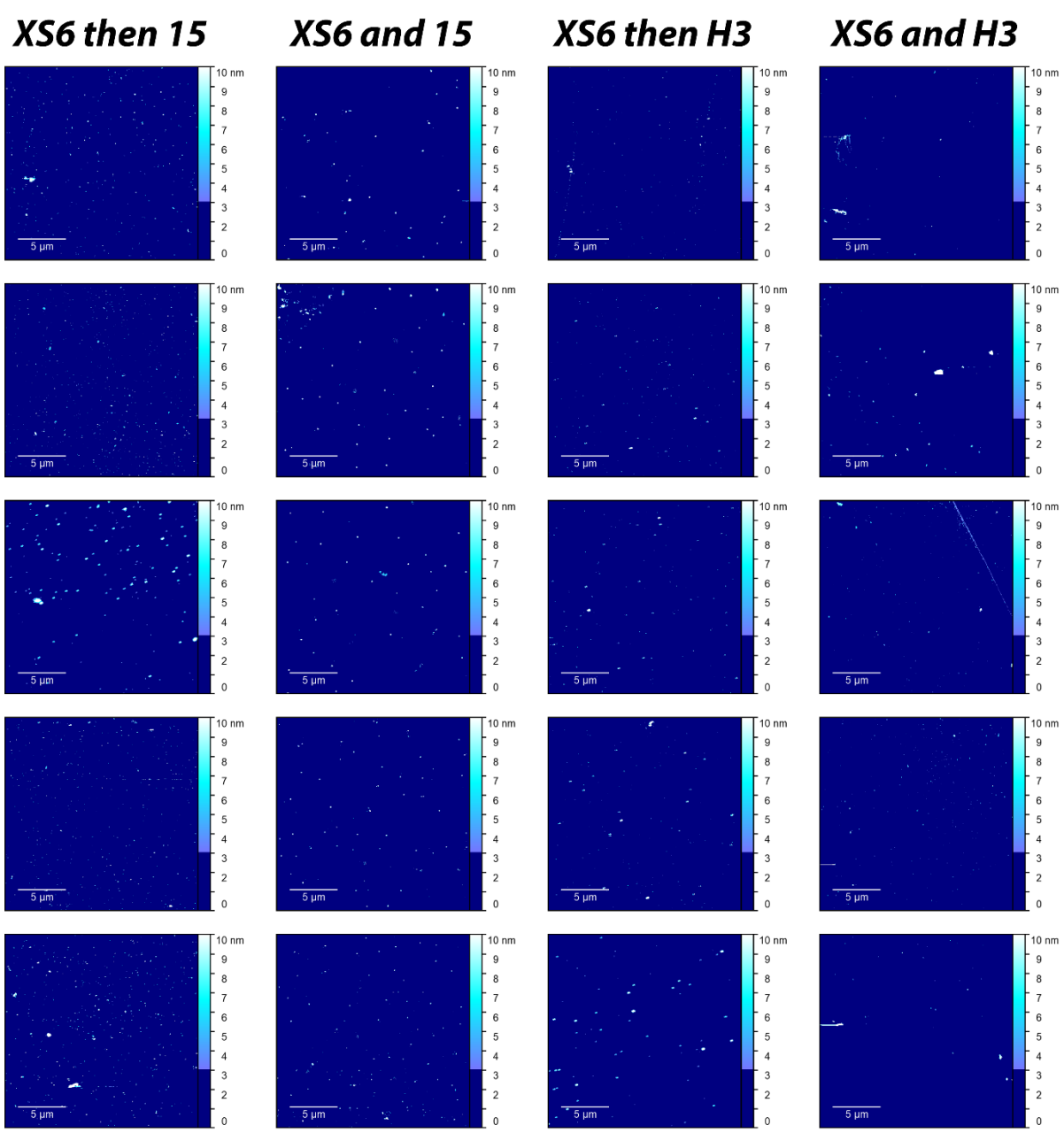
XS6 then 15
XS6 and 15
XS6 then H3
XS6 and H3
10 nm
9
8
7
6
5
4
3
2
0
5 µm

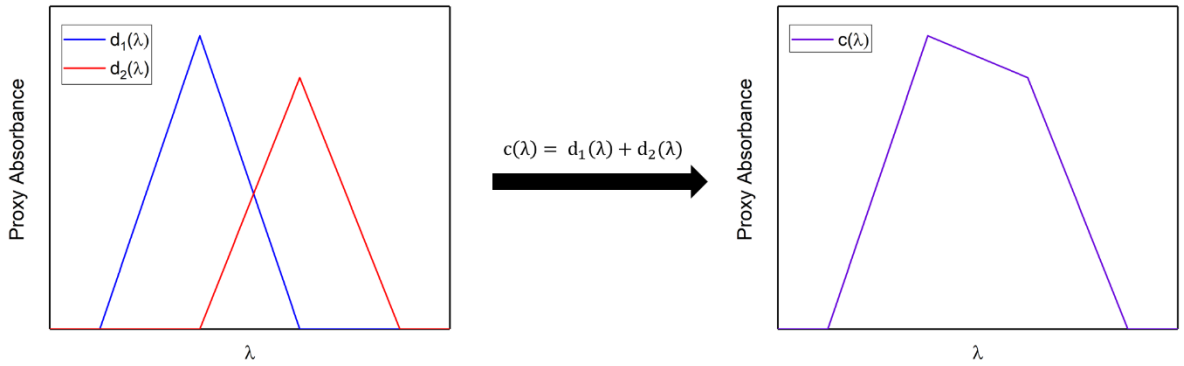

.

SI Fig. 6. The potential co-sensitization of two dyes with proxy spectra $d_1(\lambda)$ (blue) and $d_2(\lambda)$ (red) is evaluated by considering the co-sensitized proxy spectra $c(\lambda)$ (purple). $d_1(\lambda)$ has a higher extinction coefficient than $d_2(\lambda)$; however, $d_2(\lambda)$ has an optical absorption peak at a higher wavelength than $d_1(\lambda)$ making the two dyes good candidates for co-sensitization.

SI Table 1. Sequential and cocktail sensitization methods[56] employed for co-sensitizations

Sample Name	Method	Description
C1 then 15	Sequential	0.3 mM C1 for 30 min then 0.3 mM 15 for 24 hours
C1 and 15	Cocktail	0.3 mM of C1 and 15 in a 1:10 ratio for 24 hours
H3 then C1	Sequential	0.3 mM H3 for 24 hours then 0.3 mM C1 for 24 hours
C1 and H3	Cocktail	0.3 mM of C1 and H3 in a 1:3 ratio for 24 hours
8c then 15	Sequential	0.3 mM 8c for 24 hours then 0.3 mM 15 for 24 hours
8c and 15	Cocktail	0.3 mM of 8c and 15 in a 1:1 ratio for 24 hours
H3 then 8c	Sequential	0.3 mM H3 for 24 hours then 0.3 mM 8c for 24 hours
8c and H3	Cocktail	0.3 mM of 8c and H3 in a 1:1 ratio for 24 hours
XS6 then 15	Sequential	0.3 mM XS6 for 24 hours then 0.3 mM 15 for 24 hours
XS6 and 15	Cocktail	0.3 mM of XS6 and 15 in a 1:4 ratio for 24 hours
XS6 then H3	Sequential	0.3 mM H3 for 24 hours then 0.3 mM XS6 for 24 hours
XS6 and H3	Cocktail	0.3 mM of XS6 and H3 in a 1:2 ratio for 24 hours

SI Table 2. Photovoltaic performance of singly-sensitized and co-sensitized solar cells

Sample	J_{sc} (mA/cm^2)	V_{oc} (mV)	FF	$\eta^{\dagger}$ (%)	$\eta_{dye}:\eta_{N719}$	% Change
N719	**5.8 ± 0.6**	**730 ± 20**	**0.57 ± 0.02**	**2.4 ± 0.2**	**1**	**-**
C1	1.9 ± 0.2	630 ± 5	0.61 ± 0.02	0.75 ± 0.07	0.31	-
8c	0.4 ± 0.1	290 ± 50	0.46 ± 0.01	0.06 ± 0.03	0.02	-
XS6	**4.1 ± 0.8**	**730 ± 60**	**0.54 ± 0.02**	**1.6 ± 0.4**	**0.67**	**-**
15	**4.0 ± 0.5**	**640 ± 5**	**0.49 ± 0.02**	**1.22 ± 0.09**	**0.51**	**-**
H3	0.26 ± 0.01	460 ± 20	0.51 ± 0.01	0.06 ± 0.01	0.03	-
C1 then 15	3.9 ± 0.2	630 ± 5	0.53 ± 0.02	1.30 ± 0.05	0.54	6.0
C1 and 15	4.0 ± 0.5	640 ± 5	0.52 ± 0.03	1.3 ± 0.1	0.54	7.4
H3 then C1	0.6 ± 0.1	530 ± 20	0.55 ± 0.03	0.17 ± 0.06	0.07	-77.5
C1 and H3	0.48 ± 0.05	500 ± 20	0.51 ± 0.01	0.13 ± 0.02	0.05	-83.2
8c then 15	2.7 ± 0.2	480 ± 20	0.43 ± 0.02	0.57 ± 0.04	0.23	-53.8
8c and 15	3.6 ± 0.4	530 ± 50	0.42 ± 0.01	0.8 ± 0.1	0.34	-33.5
H3 then 8c	0.21 ± 0.09	270 ± 40	0.46 ± 0.01	0.03 ± 0.02	0.01	-55.4
8c and H3	0.3 ± 0.1	240 ± 40	0.45 ± 0.01	0.03 ± 0.02	0.01	-49.3
XS6 then 15	**5.5 ± 0.4**	**700 ± 10**	**0.52 ± 0.03**	**2.0 ± 0.3**	**0.82**	**22.7**
XS6 and 15	**6.5 ± 0.4**	**685 ± 5**	**0.50 ± 0.02**	**2.2 ± 0.2**	**0.92**	**38.1**
XS6 then H3	1.03 ± 0.03	570 ± 5	0.58 ± 0.01	0.34 ± 0.01	0.14	-78.6
XS6 and H3	1.0 ± 0.1	550 ± 10	0.54 ± 0.02	0.28 ± 0.05	0.12	-82.3

† Note that we tested the photovoltaic performance of singly-sensitized and co-sensitized DSSCs compared to a reference sample sensitized with the organometallic N719 dye. These are the recorded absolute η values, but it is the *relative* values given in the next column that are meaningful: reporting with the $\eta_{dye}:\eta_{N719}$ ratio method permits a far more effective comparison of power conversion efficiencies, η, than traditionally reported absolute values that have been published in the literature under a range of experimental conditions. This relative method has already been adopted in over 250 journal articles.[38]

SI Table 3. Calculated molecular dimensions and SLD values for each dye

Dye	Formula	Z	l (Å)	w (Å)	V (Å^3)	SLD_{ideal} (Å^{-2})
C1	$C_{58}H_{58}N_4O_5$	474	26.4	18.0	1120	11.9 x 10^{-6}
8c	$C_{29}H_{21}N_3O_2S_5$	312	19.6	13.5	670	13.1 x 10^{-6}
XS6	$C_{46}H_{40}N_4O_2$	360	23.1	10.1	850	11.9 x 10^{-6}
15	$C_{43}H_{37}NO_4SiS$	364	15.1	11.3	840	12.2 x 10^{-6}
H3	$C_{43}H_{43}N_5O_4S_2$	400	28.4	17.1	900	12.5 x 10^{-6}

SI Table 4. All XRR fitted parameters for singly-sensitized and co-sensitized working electrodes

Sample	Dye Layer Parameters			TiO_2 Layer Parameters		
	Thickness (Å)	**SLD x 10^{-6} (Å^{-2})**	**Surface Roughness (Å)**	**Thickness (Å)**	**SLD x 10^{-6} (Å^{-2})**	**Interfacial Roughness (Å)**
C1	43.5 ± 0.9	6.6 ± 0.5	5.6 ± 0.7	57.6 ± 0.1	30.1 ± 0.4	3.5 ± 0.1
8c	26.6 ± 0.9	5.1 ± 0.9	3.3 ± 0.8	48.9 ± 0.1	31 ± 1	4.5 ± 0.2
XS6	23.6 ± 0.5	8.7 ± 0.4	3.7 ± 0.5	58.3 ± 0.1	32.3 ± 0.5	3.6 ± 0.1
15	27 ± 1	6.7 ± 0.5	3.7 ± 0.5	57.1 ± 0.1	32.9 ± 0.7	3.9 ± 0.1
H3	24.3 ± 0.3	7.8 ± 0.4	2.7 ± 0.3	57.0 ± 0.1	30.8 ± 0.6	3.6 ± 0.2
C1 then 15	33.7 ± 0.5	5.9 ± 0.7	3.1 ± 0.6	56.9 ± 0.1	30.4 ± 0.7	3.9 ± 0.1
C1 and 15	21.5 ± 0.8	6.3 ± 0.9	3.8 ± 0.7	50.3 ± 0.1	29.0 ± 0.5	4.0 ± 0.1
H3 then C1	42 ± 1	6.0 ± 0.6	5.2 ± 0.7	57.4 ± 0.1	31.0 ± 0.5	3.7 ± 0.1
C1 and H3	25.4 ± 0.4	8.5 ± 0.4	3.0 ± 0.5	57.6 ± 0.1	32.0 ± 0.5	3.6 ± 0.2
8c then 15	30.9 ± 0.4	6.9 ± 0.4	3.9 ± 0.6	58.0 ± 0.1	34.3 ± 0.5	3.7 ± 0.1
8c and 15	31 ± 2	5.7 ± 0.5	7 ± 2	57.7 ± 0.1	36.4 ± 0.5	4 ± 1
H3 then 8c	37.2 ± 0.2	9.0 ± 0.7	2.9 ± 0.4	57.6 ± 0.1	34.2 ± 0.6	3.2 ± 0.1
8c and H3	27.5 ± 0.4	8.0 ± 0.4	3.3 ± 0.6	58.4 ± 0.1	32.0 ± 0.6	3.5 ± 0.1
XS6 then 15	**18.8 ± 0.3**	**8.7 ± 0.5**	**3.6 ± 0.4**	**57.9 ± 0.1**	**31.6 ± 0.4**	**3.9 ± 0.1**
XS6 and 15	**18.6 ± 0.3**	**8.8 ± 0.5**	**3.4 ± 0.4**	**58.2 ± 0.1**	**31.3 ± 0.5**	**3.9 ± 0.2**
XS6 then H3	21.0 ± 0.3	9.6 ± 0.5	4.1 ± 0.4	58.0 ± 0.1	31.2 ± 0.4	3.8 ± 0.1
XS6 and H3	21.6 ± 0.6	8.7 ± 0.6	4.0 ± 0.5	58.1 ± 0.1	31.3 ± 0.6	3.7 ± 0.2